Applied Catalysis B: Environmental 248 (2019) 167–183

Contents lists available at ScienceDirect

Applied Catalysis B: Environmental

journal homepage: www.elsevier.com/locate/apcatb

Ag-La loaded protonated carbon nitrides nanotubes (pCNNT) with improved charge separation in a monolithic honeycomb photoreactor for enhanced bireforming of methane (BRM) to fuels

Beenish Tahir, Muhammad Tahir, Nor Aishah Saidina Amin*

Chemical Reaction Engineering Group (CREG), Department of Chemical Engineering, School of Chemical and Energy Engineering, Faculty of Engineering, Universiti Teknologi Malaysia, 81310 UTM, Johor Bahru, Johor, Malaysia

ARTICLE INFO

Keywords:
Photocatalytic dry reforming
Bi-reforming
pCN nanotubes
Synthesis gas (CO/H_2)
Monolithic structure

ABSTRACT

Well-designed Ag-La modified protonated graphitic carbon nitride nanotubes (pCNNT) are fabricated via a template-free sonicated assisted one-pot hydrothermal method. The structure and properties of the catalyst samples are obtained by XRD, SEM, TEM, EDX, N_2-sorption, XPS, UV–vis DRS and PL spectroscopy characterization techniques. The effect of Ag-La-modified pCNNT is evaluated for different CH_4 reforming processes such as dry reforming of methane (DRM) and bi-reforming of methane (BRM), carried out in a fixed-bed and monolithic honeycomb photoreactor systems under UV and visible light irradiations. The optimized 3%Ag-5% La/pCNNT performance displayed increased productivity under UV-light due to more production of charges with strong ability for cleaving both stable CO_2 and CH_4 molecules. More importantly, the performance of Ag-La loaded pCNNT is 1.45 and 2.10 folds higher for CO and H_2 production, respectively compared with Ag-La loaded pCN nanosheets. CO and H_2 evolutions prevailed in a monolith photoreactor compared to fixed-bed reactor. Besides, the amount of CO, H_2 and CH_3OH are 1.79, 2.12 and 2.13 folds higher in BRM compared to DRM. The improved performance can be ascribed to effective interfacial carrier separation due to Ag-La synergistic effect with suitable redox potentials for BRM process. The quantum yield is significantly enhanced with BRM in the monolithic honeycomb photoreactor loaded with Ag-La modified pCNNTs due to greater photon energy utilization, larger illuminated surface area, improved sorption process and surface reactions with efficient charge carrier utilization for CO_2 reduction and CH_4/H_2O oxidation. Reaction mechanism is proposed to commensurate with the performance of Ag-La/pCNNT for BRM process based on characterization analysis and experimental results. The experimental results could provide guidance for further development of advanced and highly efficient hetero-structures for photocatalytic BRM applications.

1. Introduction

Photocatalytic reduction of greenhouse gas CO_2 seems a potential alternative to mitigate global temperature and would help to solve ecological problems with fossil fuels derived replacements. Since 1980s, water as a reductant for the reduction of CO_2 over various photo-catalysts in a gas phase and slurry system, has attracted considerable interest [1–4]. For this purpose, titanium dioxide (TiO_2) as semiconductor photocatalyst has been explored and is famous for the production of carbon monoxide (CO), methane (CH_4), methanol (CH_3OH), formic acid (HCOOH) and acetic acid (CH_3COOH) as discussed in Eqs. (1)–(5).

$$CO_2 + 2H^+ + 2e^- \xrightarrow{hv,\ catalyst,\ gas\ phase} CO + H_2O \quad (1)$$

$$CO_2 + 2H^+ + 2e^- \xrightarrow{hv,\ catalyst,\ slurry} HCOOH \quad (2)$$

$$CO_2 + 6H^+ + 6e^- \xrightarrow{hv,\ catalyst,\ slurry/gas} CH_3OH + H_2O \quad (3)$$

$$CO_2 + 8H^+ + 8e^- \xrightarrow{hv,\ catalyst,\ gas\ phase} CH_4 + 2H_2O \quad (4)$$

$$2CO_2 + 8H^+ + 8e^- \xrightarrow{hv,\ catalyst,\ slurry} CH_3COOH + 2H_2O \quad (5)$$

When CO_2 reacts with H_2O vapors in a two phase heterogeneous system (gas and solid), CO, CH_4 and CH_3OH are produced as explained in Eqs. (1), (3) and (4). It was reported that CH_4 was the main product over Fe/TiO_2 [5], CeO loaded with Fe produces CO/CH_4 [6] and CO was obtained over Ag/CdS photocatalyst [7]. Using three phase heterogeneous slurry system (gas, liquid and solid), CH_3OH, HCOOH and

* Corresponding author.
E-mail address: noraishah@cheme.utm.my (N.A.S. Amin).

https://doi.org/10.1016/j.apcatb.2019.01.076
Received 17 October 2018; Received in revised form 19 January 2019; Accepted 27 January 2019
Available online 30 January 2019
0926-3373/

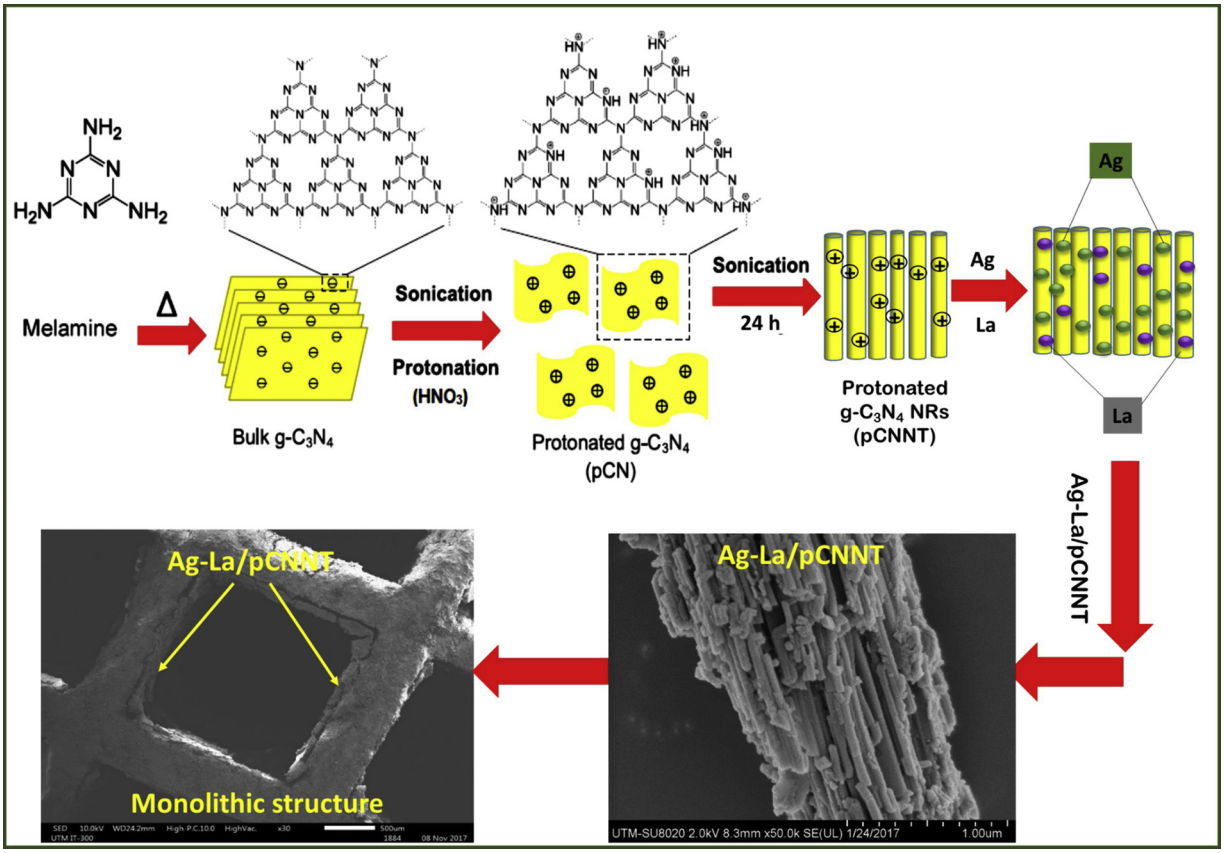

Fig. 1. Schematic of Ag-La-loaded carbon nitrides nanotubes (Ag-La/pCNNT) preparation and its coating over monolithic support.

CH_3COOH prevailed during photocatalytic CO_2 reduction with H_2O in a slurry system as explained in Eqs. (2), (3) and (5) [8]. CeO/TiO_2 conferred products mainly CH_3OH and HCHO [9], while CH_3OH and HCOOH were observed over $g\text{-}C_3N_4/Cu/TiO_2$ [10].

Although different types of photo-catalysts with appreciable improvement in CO_2 reduction to fuels has been succeeded by numerous researchers, research on recycling greenhouse gases namely CH_4 and CO_2 is still relevant. The reduction of CO_2 and CH_4 is a challenges task as both are stable molecules, while reforming of these two molecules to synthesis gas (CO, H_2) is an endothermic process that demands excessive supply of energy [11,12]. CH_4 can be converted into syngas in steam reforming of methane (SRM) as shown in Eq. (6). CO_2 can be utilized with CH_4 for the production of syngas through catalytic CO_2 and CH_4 reforming or dry reforming of methane (DRM) as explained in Eq. (7) [13]. DRM offers a number of remarkable advantages such as mitigation of both greenhouse gases, and direct production of syngas [14].

$$CH_4 + H_2O \rightarrow CO + 3H_2$$
$$\Delta H_{298K} = +206 \text{kJ/mol}$$
$$\Delta G_{298K} = +142 \text{kJ/mol} \quad (6)$$

$$CH_4 + CO_2 \rightarrow 2CO + 2H_2$$
$$\Delta H_{298K} = +247 \text{ kJ/mol}$$
$$\Delta G_{298K} = +170 \text{ kJ/mol} \quad (7)$$

However, DRM operating under higher temperature is prone to coking and reduces catalyst stability [15]. In one of the earlier studies, Shi et al. [16] reported photocatalytic CO_2 reduction with CH_4 over Cu/CdS modified TiO_2/SiO_2 photo-catalyst in a fixed-bed photoreactor operating at high temperature. Products obtained were C_2H_6, CH_3COOH, CH_3COCH_3 and CO. ZrO_2 photocatalyst was employed for CO_2-CH_4 reduction utilizing UV-light with the production of CO and H_2 as the main products [17]. Similarly, CO and H_2 were produced over Pt-loaded TiO_2 and Au/Rh loaded TNTs catalyst, respectively [18]. In all of the reports, TiO_2 is primarily considered as a promising semiconductor photo-catalyst under UV-light irradiation, while employing higher temperature. However, the amount and selectivity of the products reported are not appreciable for commercialization purposes. This is because photocatalytic CO_2 reforming of CH_4 is a challenging task depending on competent and selective photo-catalysts. Higher photoactivity is desired while the mechanisms of CO_2-CH_4 reaction system is still not well established.

Combination of SRM and DRM also known as bi-reforming (BRM) could be a promising approach and interesting pathway for production of H_2 enriched syngas as explained in Eq. (8) [19]. Bi-reforming of methane (BRM) has advantage over SRM and DRM for producing hydrogen with a stoichiometric H_2/CO ratio of 2, a more favourable composition for the production of liquid fuels via Fischer-Tropsch Synthesis (FTS) [20].

$$3CH_4 + CO_2 + 2H_2O \rightarrow 4CO + 8H_2$$
$$\Delta H_{298K} = +220 \text{ kJ/mol}$$
$$\Delta G_{298K} = +151 \text{ kJ/mol} \quad (8)$$

Although, bi-reforming of methane is an attractive approach compared to DRM, it also requires larger input energy for the production of syngas [21]. However, literature on CO_2 reduction with CH_4 in the presence of H_2O via BRM is not available, while only a few reported on CO_2 and CH_4 reduction over TiO_2 based photo-catalysts as discussed previously.

Various supports and dopant have been investigated for photocatalytic CO_2 reduction using H_2O as reducing agent. Recently, graphitic carbon nitride ($g\text{-}C_3N_4$) semiconductor has been considered for CO_2 reduction application owing to its UV and visible light responsive, low-cost synthesis and high chemical/thermal stability [22,23]. Loading rare earth elements or their oxides such as cerium (Ce) and

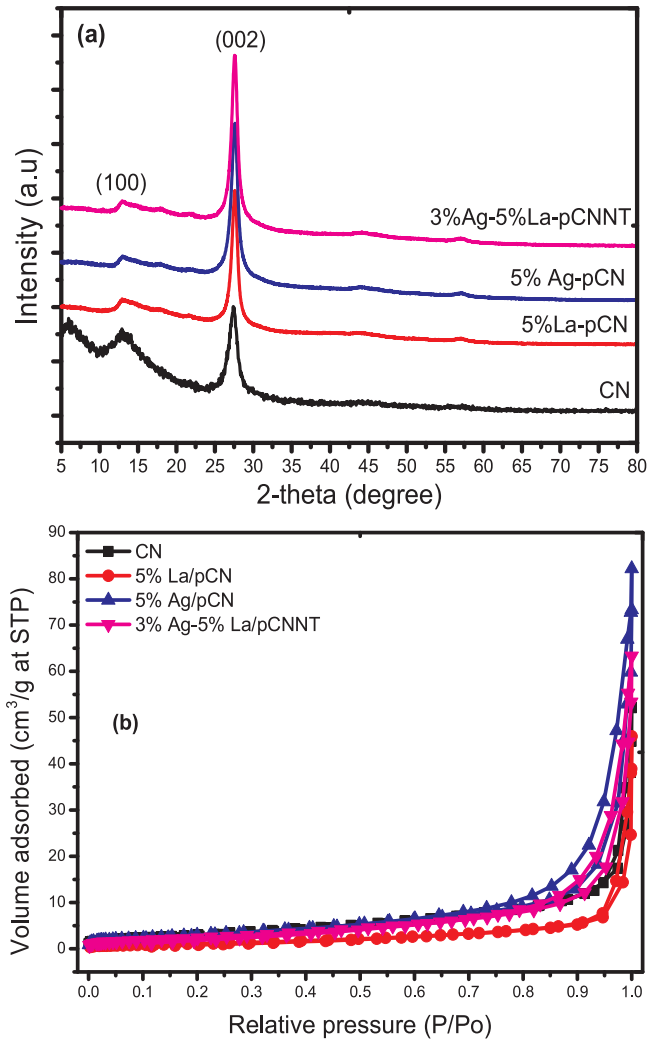

Fig. 2. (a) XRD analysis of CN and Ag-La loaded pCNNT samples; (b) N_2 adsorption desorption isotherms of CN and Ag-La modified pCNNTs samples.

Table 1
The summary of surface area and pore volume of CN and Ag-La-loaded pCNNT samples.

Catalyst	S_{BET} ($m^2 g^{-1}$)	S_{BJH} ($m^2 g^{-1}$)	BJH Pore Vol. ($cm^3 g^{-1}$)	BJH pore diameter (nm)	Band gap energy (eV)
Pristine CN	5.2	2.6	0.036	2.09	2.70
5 % Ag-pCN	12.2	16.7	0.115	2.29	2.61
5 % La-pCN	4.1	6.7	0.062	2.83	2.63
3 %Ag-5 % La/ pCNNT	8.3	14.6	0.087	2.71	2.60

lanthanum (La) is appropriate for CO_2 activation due to their basic property. CeO_2 loaded into g-C_3N_4 remarkably enhanced photocatalytic activity for CO_2 reduction by H_2O to CO and CH_4 [24]. La, with its unique electronic configuration, has been considered as a promising dopant to enhance CO_2 surface adsorption and crystal structure and optical properties [25–27]. La/TiO_2 for CO_2 reduction by H_2O was reported by Li et al. [28], for selective CH_4 production under UV-light. Similarly, better CO_2 reduction via DRM over La/TiO_2 catalyst was reported under UV-light with CO and H_2 production [29]. Ag has been investigated due to its excellent electrical conductivity, and strong electron trapping ability to enhance photo-activity [30]. For example, greater photocatalytic CO_2 reduction to fuels over Ag/TiO_2 NWs under UV was reported compared to visible light due to efficient charge separation [31]. Similarly, Ag-loaded gC_3N_4 has been investigated for selective H_2 production as Ag suppressed the recombination of charge carriers [32,33]. Ag-modified TiO_2 loaded over monolithic support for dynamic photocatalytic CO_2 reduction under UV-light has been reported to hinder recombination of photo-generated electron-hole pairs [34]. Graphene bridged TiO_2 loaded with Ag-nanocubes was found efficient for photocatalytic CO_2 reduction since rGO/Ag co-loading facilitates the transfer of electrons, leading to enhance photo-activity [35]. Meanwhile, significantly improved photo-activity was also observed due to efficient trapping of electrons by Ag in TiO_2 nanotubes during photocatalytic CO_2 reduction with H_2O [36]. Similarly, Ag-loaded g-C_3N_4/TiO_2 for CO_2 photo-reduction by H_2O to fuels was explored [37]. g-C_3N_4 is widely investigated in photocatalytic CO_2 reduction with H_2O, but not for CO_2-CH_4 reaction system via DRM and BRM. The efficiency of g-C_3N_4 can be further improved through surface charge modification via protonation [38]. In addition, loading Ag and La into protonated g-C_3N_4 is desired to enhance both photoactivity and products selectivity.

Structured nanomaterials such as nanosheets, nanotubes and nanowires have been demonstrated to have potential for faster transportation of electrons due to hinder recombination rate [38–40]. Among them, one dimensional (1D) nanotubes not only provide a short diffusion length, but also quick transport electrons along their axis [41]. However, limited reports are available on the fabrication of 1D g-C_3N_4 nanotubes. In addition of efficient photo-catalysts, reactor configuration also contributed to improving efficiency and productivity. Among structured supports, monolith has been investigated for enhanced and selective CO_2 reduction with H_2O over TiO_2 based photo-catalysts [34,42]. Thus, photocatalytic CO_2 reduction with CH_4 via BRM process would be potentially a workable approach. Furthermore, the fabrication of one dimensional (1D) nanomaterial can provide large surface area with regular structure, thus enriching photo-generated charge transport and hindering charge recombination rate. Up to now there is no report on DRM and BRM reforming processes using La/Ag modified graphitic carbon nitride nanotubes photocatalyst loaded over the monolithic support.

Herein, protonated graphitic carbon nitride nanotubes (pCNNT) modified with Ag-La and loaded over monolithic support was prepared. The performance of the photocatalyst with faster charge separation was tested for CO_2-H_2O photo-reduction with CH_4 via BRM for the production of synthesis gas. The samples were synthesized using a template free sono-hydrothermal assisted photo-deposition approach. The effect of Ag-La modified pCNNT was explored under various reaction systems; for example, CO_2 photo-reduction with H_2O, steam reforming of methane (SRM), dry reforming of methane (DRM) and bi-reforming of methane (BRM) to maximize production rate. The effect of reductant type, irradiation type, reaction time and types of reactor on the photocatalytic activity of Ag-La/pCNNT was critically investigated. In particular, the performance of Ag-La-loaded pCNNT catalysts was tested in a fixed-bed and monolith photoreactor under UV and visible light irradiations to get higher production rate of synthesis gas. The quantum efficiency was calculated for different reforming systems under UV and visible light irradiations in a fixed- bed and monolith photoreactor for determining products evolved based on the utilization of photonic flux. In addition, reaction mechanism for photocatalytic BRM over Ag-La/pCNNT was proposed based on the experimental results.

2. Experimental

2.1. Preparation of Ag-La loaded pCNNT

The bulk graphitic carbon nitride (g-C_3N_4) was prepared by the thermal decomposition of melamine (Sigma Aldrich AR ≥ 99%). Typically, 5 g of melamine placed in a crucible was heated to 550 °C @

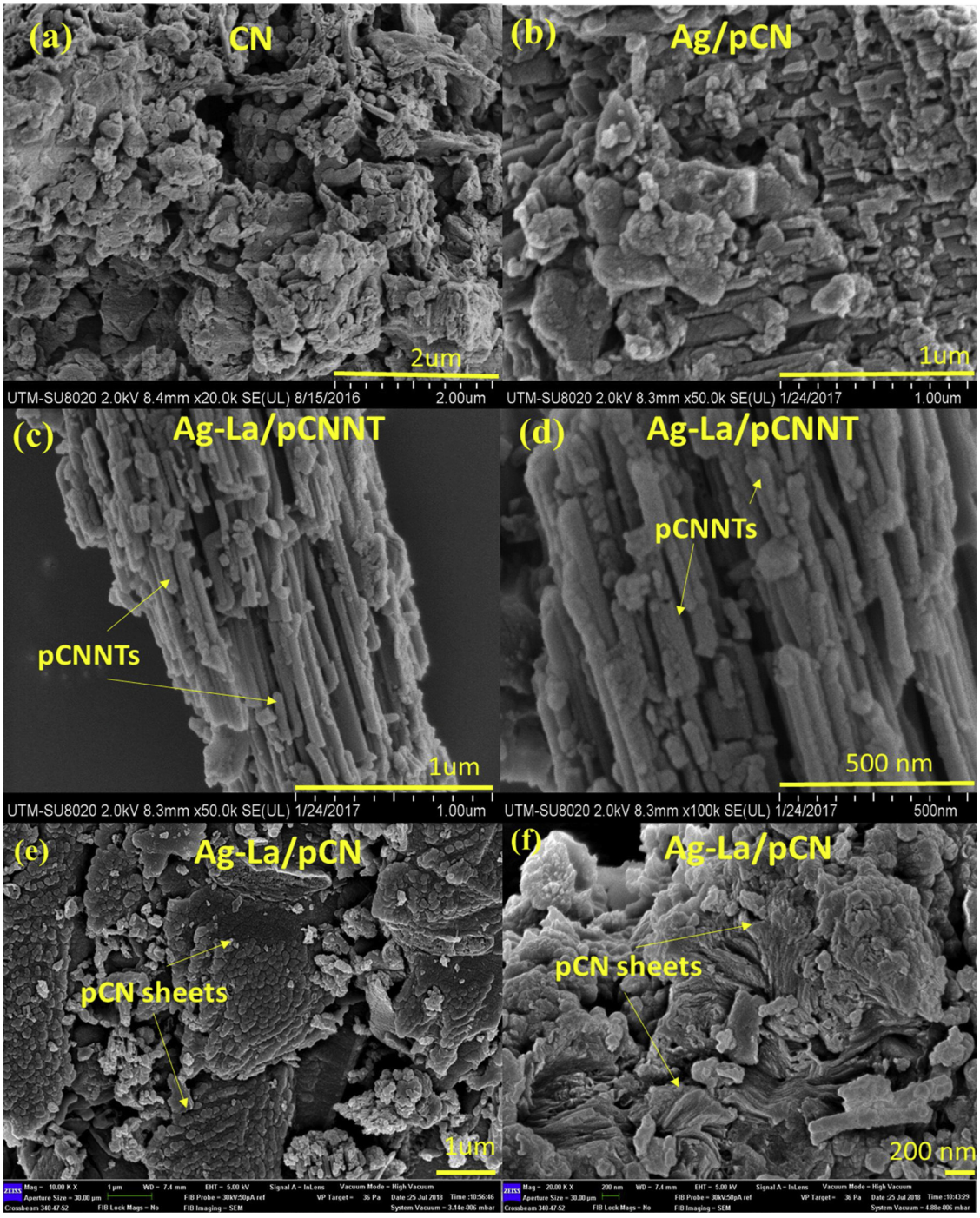

Fig. 3. FESEM analysis of pristine CN and 3% Ag-5% La-loaded pCNNT samples: (a) pristine CN, (b) 5% Ag/pCN, (c–d) 3% Ag-5% La/pCNNT, (e–f) 3% Ag-5% La/pCN.

5 °C/min for duration of 2 h and the g-C_3N_4 powder obtained was a light yellow color. The bulk g-C_3N_4 was grounded to get fine powder using Mortar and pestle and was further used for the surface charge modification via protonation with nitric acid solution. Typically, 1 g g-C_3N_4 powder was immersed in nitric acid solution (0.1 M) by stirring for 24 h; afterwards, slurry was filtered and sludge obtained was washed with distilled water. The sample obtained was dried at 110 °C in the oven under air flow for 12 h. The pristine g-C_3N_4 and protonated carbon nitrides were denoted as CN and pCN, respectively.

Next, for La-loading, an appropriate amount of $LaNO_3$ dissolved in water was added into the pCN solution, sonicated for 30 min, stirred for 6 h and finally sonicated for 30 min. The obtained sludge was centrifuged, oven dried at 110 °C for 12 h and finally named as La/pCN samples. Similarly, for the preparation of Ag/pCN samples, Ag-NPs were loaded over the pCN samples via the sonication and photo-deposition method, alternatively. For this purpose, specific amount of pCN was dispersed in 20 mL water and specific amount of Ag $(NO_3)_2$ $3H_2O$ was added to it, sonicated for 30 min, stirred for 6 h and finally sonicated for 30 min at room temperature. Finally, samples were UV-irradiated for 15 min to get Ag-NPs loaded pCN samples.

For preparation of Ag-La co-loading carbon nitride nanotubes, both the solutions were mixed together, sonicated for 60 min and stirred for 24 h. Finally, the samples were oven-dried at 110 °C for 12 h. The resulting products obtained were Ag-La loaded protonated carbon nitrides

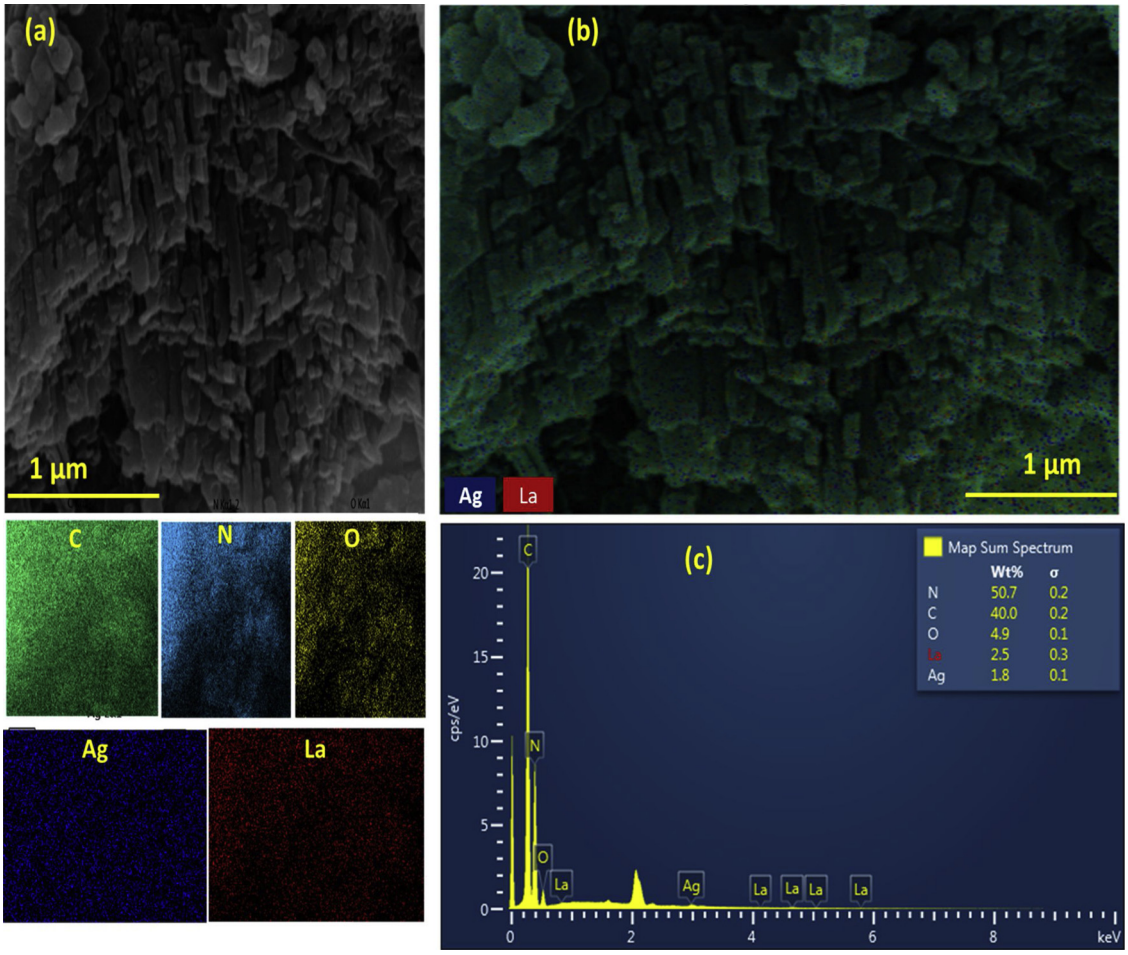

Fig. 4. (a) SEM image of Ag-La/pCNNT, (b) mapping analysis of Ag-La/pCNNT sample, (c) Spectrum of elements presents in 3% Ag-5% La/pCNNT sample.

nanotubes known as Ag-La loaded pCNNT. Different Ag-loading into 5% La/pCNNT samples were prepared by varying the amount of Ag-contents 1, 3 and 5 wt. %. Ag-La loaded pCN samples were prepared similarly except no sonication was used.

2.2. Preparation of Ag-La/pCNNT loaded over monolithic honeycomb support

The monolithic support used in this study has square straight channels with length/width 1.54 nm. The wall thickness of monolith channels is 0.64 nm and catalyst film thickness of ˜20 µm. The monoliths are made of ceramic with elements Si, Mg, Al and O. Prior to being coated over the monolithic honeycomb support, Ag-La loaded graphitic carbon nitrides nanotubes (Ag-La/pCNNTs) was dispersed in methanol under sonication for 60 min. The monolithic channels with cell density 100 CPSI (cells per square inch) were square in shape and has the dimensions of 60 mm × 60 mm (length × width) and 15 mm (height). Initially, the monoliths were cut to the desired sizes and then washed with acetone and isopropanol, alternatively, to remove any organic impurities. Finally, the weight of the bare monolith was recorded after air drying at 110 °C for 24 h. For catalyst loading, the monoliths were dipped in Ag-La/pCNNT catalyst solution and kept for 10 s. The dip excess solution was blown off using compressed air. The coating procedure was repeated several times until the desired loading of the catalyst was obtained. Finally, the monolith supported Ag-La/pCNNT catalyst was oven dried at 110 °C overnight and final weight was calculated. The schematic for the preparation of Ag-La/pCNNT coated on the monolithic support is presented in Fig. 1.

2.3. Characterization analysis

A Bruker diffractometer (D8, 40 kV, 40 mA) with a Cu Kα radiation source was used to measure X-ray diffraction (XRD) patterns to identify the crystalline structure of the samples. The analysis was conducted in a 2–θ range of 5° to 80°, with 5 s counting time. The BET surface area and pore size distribution was investigated using Thermo Scientific, SURFAR analyser, operating at −196°C. Before N_2 sorption process, all the samples were vacuum dried at temperature 250 °C for duration of 4 h. The morphological and structural analysis was conducted on a Hitachi SU8020 field emission scanning electron microscopy (FE-SEM) and HITACHI HT7700 high-resolution transmission electron microscope (HR-TEM). The composition and metals distribution was obtained using Energy-dispersive X-ray spectroscopy (EDX) analysis. The XPS (X-ray Photoelectron Spectroscopy) analysis was conducted on Axis Ultra DLD Shimadzu instrument. The deconvolution of elements was conducted using internal standard of C1s signal at 284.60 eV. UV–vis DR (diffuse reflectance) absorbance spectra were attained using spectrophotometer Cary 100 Agilent equipped with integrated sphere. Photoluminescence (PL) spectra were conducted using a Raman Spectrophotometer (HORIBA Scientific) with laser emitting wavelength of 325 nm.

2.4. Photocatalytic measurement

For fixed-bed reactor, the CO_2 photo-reduction with CH_4 experiments in the presence of water were conducted in a stainless steel photoreactor of total volume 210 cm^3. An amount of 150 mg catalyst was distributed evenly at the bottom of reactor chamber. For the

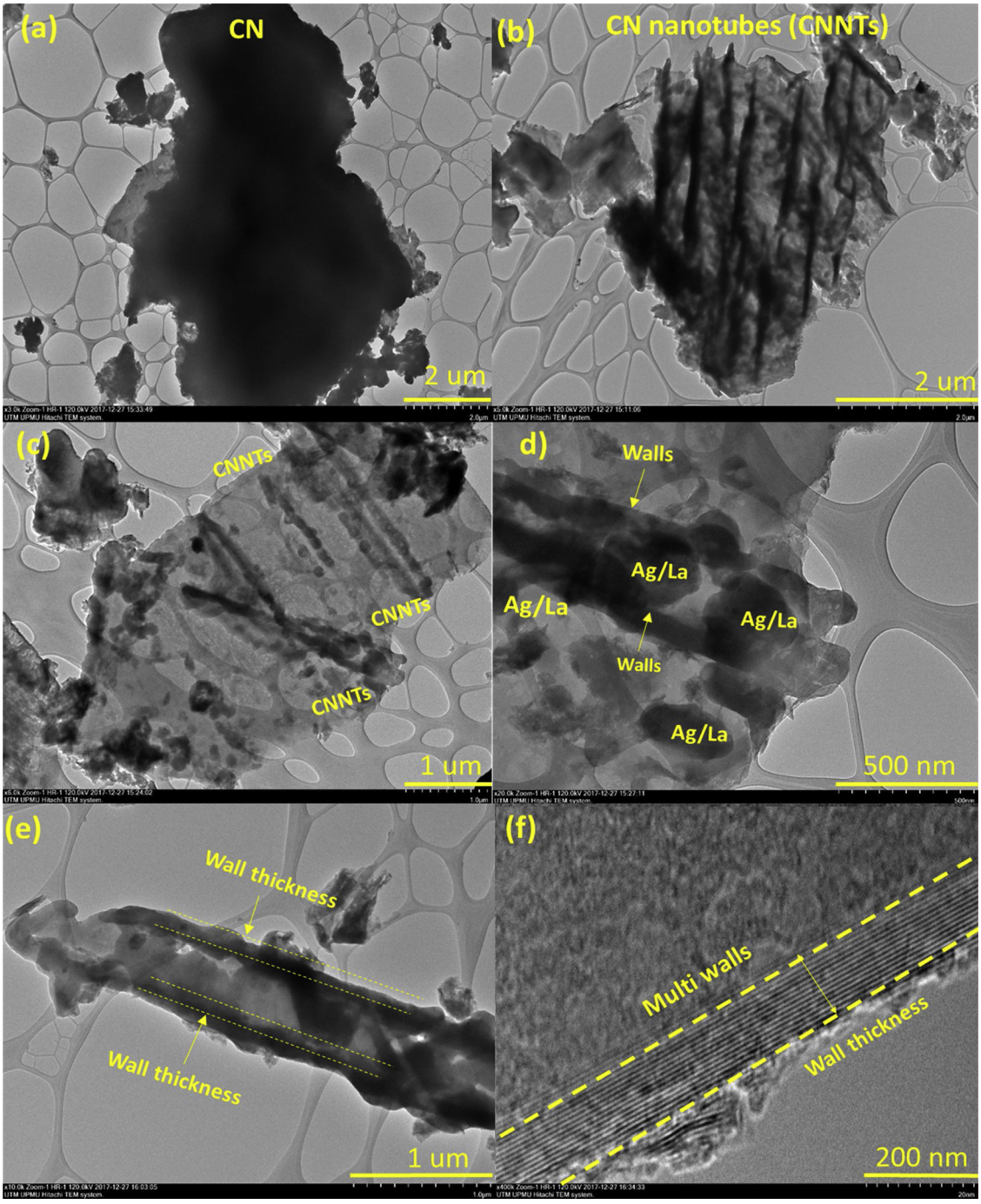

Fig. 5. TEM images of 3% Ag-5% La modified pCNNT: (a) bulk CN, (b–c) bundle of CN nanotubes, (d–e) single CN nanotube loaded with Ag-La NPs, (f) HRTEM image presenting fringes of multiwall in CN nanotubes.

monolith photoreactor system, instead of powder, catalyst coated monoliths were placed at the center of the reactor chamber as discussed in our previous work [43]. Two types of light source were used in the experiments. The UV-light source was a 200 W Hg lamp having wavelength 254 nm and light intensity 150 mW cm^{-2}. Meanwhile, the visible light source was a solar simulator LCS-100 (Newport) having 100 mW cm^{-2} light intensity and integrated with UV-cut filters. UV lamps was fixed at the top of quartz window of 8 mm thickness and provided with cooling fans to remove lamp heat. For visible light analysis, the reactor was placed under light irradiation source from solar simulator of fixed height giving light of one solar spectrum.

Compressed CO_2 (99.999%) and CH_4 (99.999%) gases regulated by mass flow controllers (MFC) were continuously passed over the catalyst. Initially, feed gases were streamed through the reactor for 30 min to saturate the catalyst and to purge the reactor prior to start experiment. Furthermore, for photocatalytic DRM process, CH_4/CO_2 molar feed ratio of 1.0 was fixed, at a total flow rate 5 mL min^{-1}. Similarly, for BRM reduction process, CO_2 was constantly flowed through the water saturator to carry moisture under water vapor pressure 0.032 bars and finally mixed with CH_4 with a total inlet flow rate of 5 mL min^{-1}. The reaction was conducted under atmospheric pressure and constant temperature 100 °C. All the products were analyzed using an on-line gas chromatograph (GC-Agilent Technologies 6890 N, USA) connected to reactor. GC was equipped with FID detector with HP-PLOT Q capillary column and TCD-detector with Porapak Q and Molecular Sieve MS-5A columns.

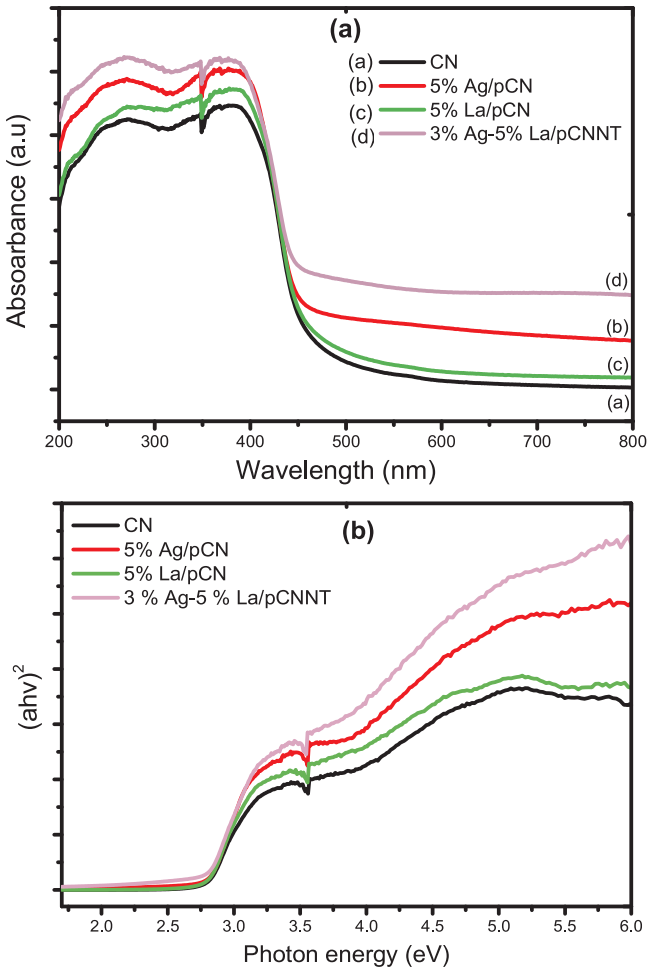

Fig. 6. (a) UV–vis diffuse reflectance absorbance spectra of CN and Ag-La-loaded pCNNT samples; (b) Plots of $(ahv)^2$ vs photon energy (eV) for band gap energy calculation.

3. Results and discussion

3.1. Characterization of catalysts

Fig. 2(a) depicts XRD patterns of pristine CN, pCN and Ag-La modified pCNNT samples. Similar to pristine CN, all Ag-La modified pCNNT samples exhibit two peaks appearing at 2-theta of 12.96° and 27.47°, corresponding to (100) and (002) crystal planes (JCPDS 87–1526) and presents successful development of graphitic carbon nitride structure. In addition, 2θ peak at 27.47° shows interlayer stacked structure; however, another peak at 2θ of 12.96° presents the intra-planar packing structure. The peaks of Ag-La in pCNNT were not identified possibly due to lower loading or these species are highly dispersed over the pCNNT structure [44].

The BET surface area of the polymeric CN and Ag-La-modified pCNNT samples are investigated using nitrogen isotherms and the results are presented in Fig. 2(b). Obviously, sorption isotherms present type IV classification with H_3 hysteresis loops. These types of loops infer the materials may have mesoporous structure. The specific surface areas and pore volumes of all the samples are listed in Table 1. The BET surface area of 5.2 $m^2 g^{-1}$ for CN increases to 12.2 $m^2 g^{-1}$ in 5% Ag/pCN sample. However, in the case of 5% La/pCN sample, the BET surface is slightly reduced (4.1 $m^2 g^{-1}$). With Ag and La co-loading, there is no significant effect on BET surface area but the mesoporous surface areas are enlarged. On the other hand, pore volume of 0.087 cm^3/g was obtained for Ag-La/pCNNT sample, somewhat, higher than pCN and La/pCN samples but lower than Ag/pCN samples. However, pore diameter was lower than La/pCN and higher than Ag/pCN and CN samples, respectively. Similar observations have been reported previously [45].

Fig. 3 exhibits FESEM images of pristine and modified CN samples. SEM image in Fig. 3(a) shows that pure CN layers are stacked together with irregular folding like structures and similar observation has been reported previously [46]. Meanwhile, after protonation with Ag-loading, pCN compact sheets-like structure are obtained as depicted in Fig. 3(b). With further sonication and addition of Ag-La, sheet-like wrapped together to obvious nanotubes (Fig. 3(c–d)). More importantly, when only stirring is used without sonication, only compact sheets of CN loaded with Ag-La are obtained as presented in Fig. 3(e–f). Therefore, successful fabrication of pCN nanotubes are obtained assisted by sonication instead of using only stirring. Fig. 4(a–b) presents EDX mapping analysis of Ag-La modified pCNNT sample. Evidently, Ag-La metals are uniformly distributed over the structured pCNNT surface. The EDX plot of elements in Fig. 4(c) confirms the presence of C, N O, Ag, and La elements in 3% Ag-5% La/pCNNT sample. Therefore, it is obvious, adding metals does not alter pCN nanostructure and are uniformly distributed over the surface to promote adsorption and charges separation.

Fig. 5 presents HRTEM analysis of pCNNT loaded with Ag and La. The bulk pCNNTs are shown in Fig. 5(a), while the presence of nanotubes is observed in Fig. 5(b–c). Fig. 5(d–e) depicts uniform size and single-shape nanotube of pCN. Evidently, Ag/La metals are distributed over the entire surface of pCNNT. The deposition of Ag/La NPs would be helpful to trap electrons. Furthermore, the nanotubes are found to be multiwall as presented in Fig. 5(f). These observations confirm that multiwall pCNNT could be produced using solvent based sonication approach, while uniform deposition of metals could be achieved using photo-deposition method.

Fig. 6(a) exhibits UV–vis diffuse reflectance absorbance spectra of pristine CN and Ag-La-modified pCNNT samples. The pristine CN and La and Ag-modified pCN samples present a similar absorption edge at around 450 nm but more light absorption could be seen in Ag-La co-modified pCNNT samples. The band gap energy, for all the samples, calculated using plot of $(ahv)^2$ versus photon energy (eV), is presented in Fig. 6(b) and summary of band gap energy is presented in Table 1. The band gap energy of pristine CN shifts from 2.70 to 2.63 eV in pCN samples. Ag-La modified pCNNT samples confers a similar band gap value in the range of 2.60 to 2.63 eV. Since, no significant shift in the band gap energy of pCN, Ag-La are not incorporated into the pCNNT crystal lattice, but dispersed evenly over the surface of pCNNT to enhance photo-activity.

Fig. 7 presents XPS analysis of Ag-La modified pCNNT photocatalyst sample. Fig. 7(a) presents wide spectra of the sample. As shown in Fig. 7(b), two La3d peaks with two groups of doublet peaks were obtained, an indicative of two bounding states. The main peaks with binding energies appeared at 835.80 eV ($3d_{5/2}$) and 852.31 eV ($3d_{3/2}$) with spin orbit splitting level of 16.51 eV. The two peaks with binding energies 839.01 and 855.76 eV present satellite peaks of $La3d_{5/2}$ and La $3d_{3/2}$, respectively. The separation difference between $3d_{5/2}$ main peak and $3d_{5/2}$ satellite peak is approximately 3.21 eV, consistent with the reported values of La^{3+} compound. This dynamic formation and decomposition of complex could be helpful for enhancing CO_2 conversion to CO through the involvement of electrons and holes [47]. Fig. 7(c) demonstrates two peaks assigned to $Ag3d_{3/2}$ and $Ag3d_{1/2}$ with binding energies 368.45 and 374.38 eV, respectively. These peaks indicate the presence of silver as Ag^{2+} state. The N1 s peaks appeared at 398.22 and 400.63 eV as shown in Fig. 7(d), appointed to C=N–C and C-NH_2 from the precursor of CN, respectively. The O1 s spectrum in Fig. 7(e) reveals a wide symmetric peak with binding energy 533.21 eV, attributed to CO_3^{2-}. Fig. 7(f) discloses C1 s peaks with binding energies 284.60 and 288. 01 eV, corresponds C–C and N–C–N functional group, respectively [45].

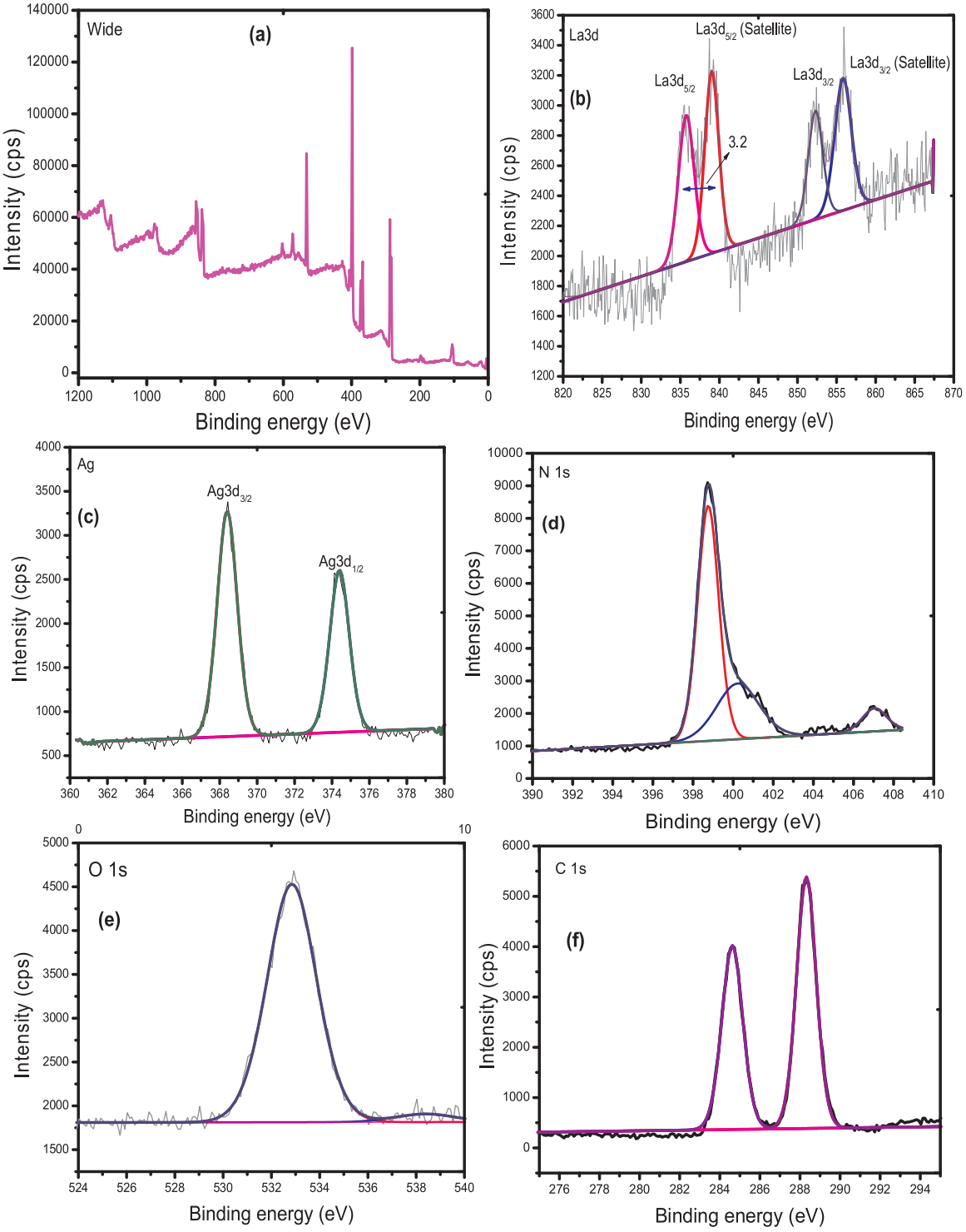

Fig. 7. XPS analysis of 3% Ag-5% La/pCNNT catalyst: (a) wide spectra, (b) La3d, (c) Ag 3d, (d) N 1 s, (e) O 1 s and (f) C 1 s.

The band structure of photo-catalyst including band gap energy, valence and conduction band positions are estimated from XPS analysis and UV–vis spectroscopy. The valence band edge of composite is evaluated from XPS survey spectra. The raw data is first normalized against the carbon C1s position at 284.60 eV and results are plotted as shown in Fig. 8(a). The intersection point of two lines corresponding to X-axis gives the valence band (VB) edge of 3% Ag-5% La-loaded pCNNT, which is 1.48 eV. The conduction band (CB) position can be evaluated using Eq. (9).

$$E_{VB} = E_{CB} + E_{bg} \quad (9)$$

where E_{VB} and E_{CB} are valence and conduction band potentials, respectively while E_{bg} is band gap energy of Ag-La/pCNNT sample. After substituting the values of E_{VB} and E_{bg} in Eq. (9), the value of E_{CB} is found to be -1.12 eV. The value is suitable for CO_2 reduction applications and similar values have been reported in the literature [48].

The charges recombination rate over CN, pCN, Ag-La/pCN and Ag-La/pCNNT samples was identified using photoluminescence (PL) analysis. Fig. 8(b) presents recombination and/or separation of photo-induced charge carriers in different samples obtained with 325 nm

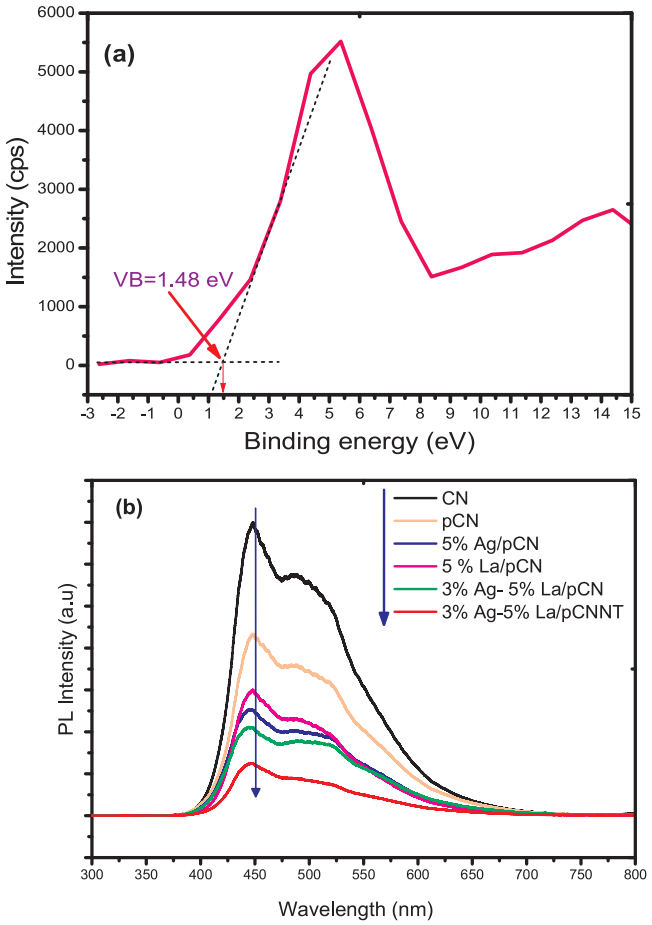

Fig. 8. (a) Calculation of VB position of 3% Ag-5% La loaded pCNNT using XPS wide spectra; (b) Photoluminescence analysis of CN, pCN and Ag-La modified pCNNT samples.

excitation wavelength and highest emission peak was observed at 516 nm. Obviously, the PL intensity is reduced in pCN compared with CN. Similarly, the emission intensity of PL spectrum for pCN photo-catalyst decreases with Ag and La-loading. Thus, the Ag-La loaded pCNNT has much lower recombination rate of photo-generated charge carriers. More importantly, Ag-La loaded pCNNT has lower intensity than Ag-La modified pCN sheets, confirming nanotubes have lower charge recombination rate due to 1D structure.

3.2. Photocatalytic CO_2 reduction with CH_4 in presence of H_2O

3.2.1. Effect of protonation and Ag-La loading on CN performance

The effect of protonation on the performance of carbon nitrides (CN) under simulated visible light for photocatalytic BRM process towards CO, H_2 and CH_3OH production is depicted in Fig. 9. It is evident that pCN registers higher photo-activity compared to pristine CN as depicted in Fig. 9(a).

Using pristine CN, the main products detected were CO and H_2 with smaller quantities of C_2H_6 and CH_3OH. The highest amount of CO produced over pCN is 165 μmole/g-cat, a 1.15 folds than the CO produced over the pristine CN photo-catalyst. On the other hand, the highest amount of H_2 of 64 μmole/g-cat is produced over the pCN photo-catalyst which is 1.10 times the amount of H_2 produced over pristine CN. Remarkably, pCN significantly increased CH_3OH amount ˜ 3.9 fold higher than the amount produced over CN photo-catalyst. These results reveal that the production of electrons and holes over the surface of pristine CN catalyst is not effectively utilized owing to the narrow band structure of CN. Thus, protonation has significant contribution to enhance photocatalytic performance of CN, obviously due to effective hindrance of charge recombination rate resulting in greater photo-activity as evident in PL analysis.

The effect of different Ag-loading on the performance of pCN is discussed in Fig. 9(b). The amounts of both CO and H_2 increase with Ag-loading and the highest amount of products are detected with 5 wt. % Ag-loaded pCN photo-catalyst. Similarly, Ag-loaded pCN catalyst also promotes CH_3OH production. Therefore, Ag/pCN samples are favourable for significant amount of H_2 and CH_3OH in addition of CO evolution. The enhanced pCN photoactivity in the presence of Ag is due to polymeric structure with hindered charges recombination rate and increased mobility of charges.

Fig. 9(c) presents the performance of La/pCN photo-catalyst samples for the evolution of CO, H_2, CH_3OH and C_2H_6 during photocatalytic CO_2 and CH_4 reforming. Noticeably, La-loading into pCN, promoted CO production, while amounts of H_2 and CH_3OH was somewhat affected. Besides, optimal La-loading amounts of 5 wt. % was obtained, producing highest amount of CO. These observations confirm that DRM process efficiency towards CO production can be increased with La-loading into pCN. Fig. 9(d) presents the effects of Ag-La co-loading on the performance of pCN photocatalyst. The main products detected are the same with Ag and La co-loading, but the formation trends are different with various amounts of Ag loading. It is observed that the production of CO and CH_3OH significantly increased with Ag and La co-loading and the highest amounts of products are detected over 3% Ag-5% La/pCNNT photocatalyst. Due to better CO_2 uptake, basic pCN and faster charge carrier separation by Ag-La, production of CO was greatly improved. Therefore, this composite was further investigated to study the effect of irradiation time, type of reductants, type of light irradiations (visible and UV-light) and effects of reactor types.

3.2.2. Effect of type of light irradiation and reductant type on Ag-La/pCNNT activity

The effect of UV and visible light irradiations and CH_4/H_2O reductants on the performance of Ag-La-loaded pCNNT for photo-induced CO_2 reaction systems in a fixed-bed reactor is shown in Fig. 10. The production of CO and H_2 under UV and visible light irradiations during photocatalytic DRM reforming process is discussed in Fig. 10(a). Under both types of light irradiations, amount of CO is larger than H_2 produced. Initially, highest amount of CO is obtained, but it declines over the time on stream and trends are consistent in both irradiations types. The reduced CO production within the irradiation time is due to decreased concentration of adsorbed CO_2 on the catalyst surface. More interestingly H_2 is continuously produced over the entire irradiation time, probably, due to the surface reactions of CH_4 with holes due to very strong basicity of Ag-La/pCNNT. More importantly, production of CO and H_2 are higher under UV-light irradiations than using visible light. This could be explained based on the strength of light intensity for breaking stable molecules. As both CO_2 and CH_4 are stable compounds and their reduction requires more light intensity with more penetration power.

The effect of H_2O reductant on the efficiency of 3% Ag-5% La-loaded pCNNT catalyst for photocatalytic CO_2 reduction with CH_4 to CO and H_2 under UV and visible light irradiations is exhibited in Fig. 10(b). Interestingly, the trends for CO productions in CO_2-CH_4-H_2O reaction system via BRM are somewhat different from the DRM system. The production of CO is enhanced by adding H_2O in DRM reaction system under both types of light irradiations. This could be probably due to H_2O is also adsorbed over the catalyst surface and promoted CO_2 reduction to CO instead of CH_4 oxidation to H_2 and C_2H_6. However, decreasing CO production over the irradiation time could be attributed to lower concentration of adsorbed CO_2 on the catalyst surface. The production of CH_3OH in CO_2-CH_4 via DRM and CO_2-CH_4-H_2O via BRM reaction systems under UV and visible light irradiations are presented in Fig. 10(c). The production of CH_3OH with CO_2-CH_4 is not much affected by adding H_2O under UV-light irradiations. However, CH_3OH

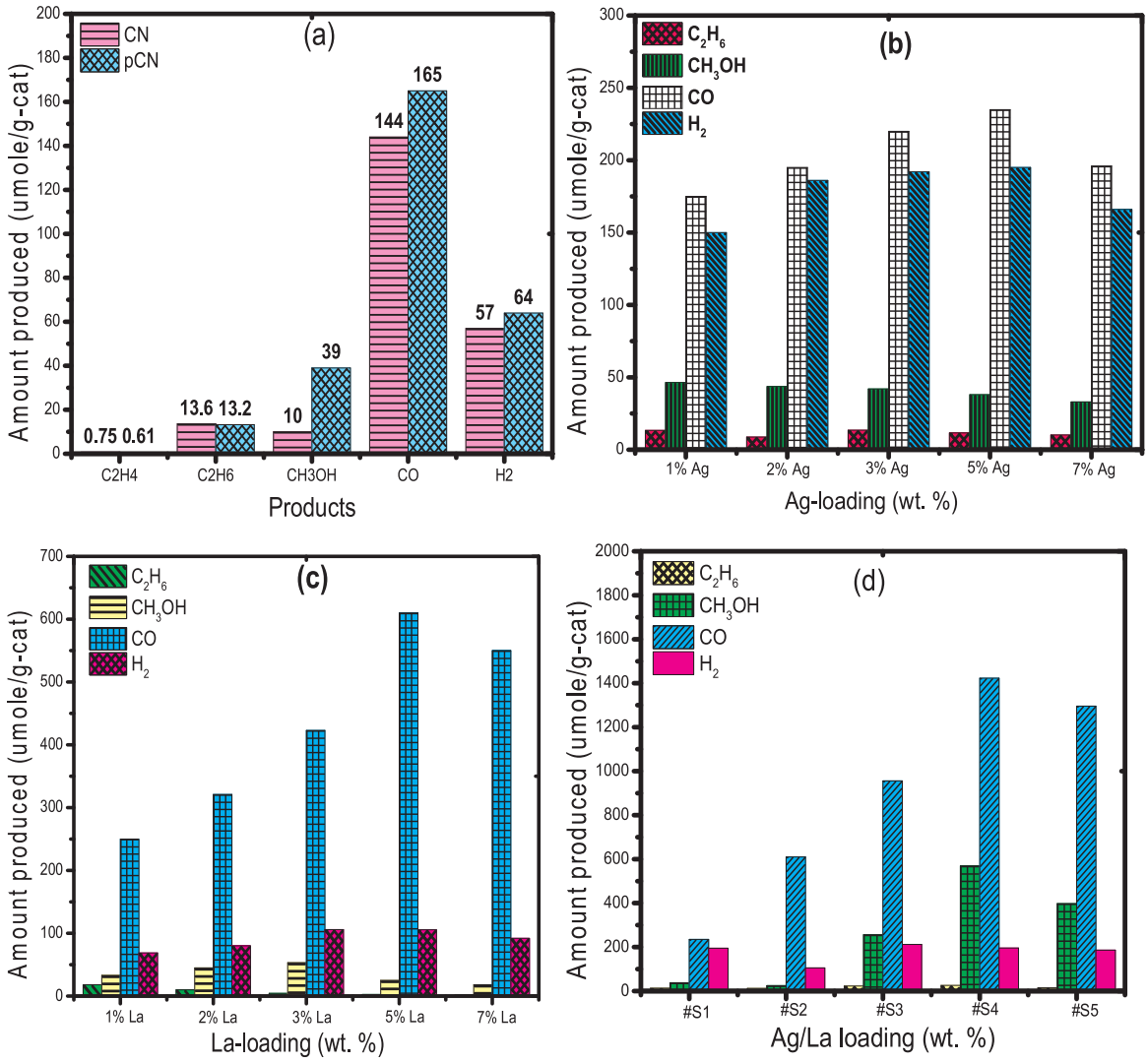

Fig. 9. Effect of Ag-La loading on the performance of pCN photocatalyst for CO_2 reduction with CH_4 in a fixed-bed reactor under visible light at temperature 100 °C and time 2 h: (a) effect of protonation; (b) Ag-loading, (b) La-loading, and (d) Ag-La loading to pCNNT: #S1 5%Ag/pCN, #S2 5% La/pCN, #S3 1% Ag-5% La/pCNNT, #S4 3% Ag-5% La/pCNNT, #S5 5% Ag-5% La/pCNNT.

production is enhanced by adding H_2O in CO_2-CH_4 reaction system under visible light irradiation. Higher CH_3OH production under visible light could be attributed to lower light intensity, which is not strong enough for CH_3OH reduction. The highest amount of C_2H_6 is produced using CO_2-CH_4 via DRM and CO_2-CH_4-H_2O via BRM reaction systems under UV-light irradiations as depicted in Fig. 10(d). This is perhaps due to the cleavage of CH_4 in the presence of La for the production of C_2H_6. In general, enhanced efficiency of Ag-La-loaded pCNNT could be due to enhanced CO_2 adsorption with larger surface area and hindered charge recombination rate.

The schematic presentation of photocatalytic BRM over Ag-La modified pCNNT photocatalyst under visible light and UV-light is presented in Fig. 11. According to experimental results, the performance of photocatalyst under UV-light is much better than using visible light irradiations. Fig. 11(a) presents CO_2 and CH_4 reforming under visible light irradiations due to photocatalyst functional under visible light. Thus, the photoactivity under visible light over g-C_3N_4 is due to its appropriate band gap structure and trapping of electrons by Ag-La. The photoactivity of Ag-La/pCNNT under UV-light for bi-reforming of methane is presented in Fig. 11(b). The UV-light used has wavelength of 254 nm which is suitable to activate Ag due to its d-band of 4.26 eV, lower than the band energy of the UV-light. Thus, Ag would be activated under UV-light irradiations transferring electrons to activate pCNNT. At the same time, Ag-La would be suitable for trapping electrons. The combined effects of Ag-La co-loading with pCNNT under UV-light irradiations promotes the photoactivity for the production of CO, H_2 and hydrocarbons.

3.2.3. *Effect of morphology on the pCN performance*

The effect of 3% Ag-5% La co-loading in pCNNT for photocatalytic CO_2 reforming of CH_4 in the presence of H_2O is illustrated in Fig. 12(a). Evidently, 3% Ag-5% La/pCNNT registers higher photo-activity compared to 3% Ag-5% La/ pCN sheets, and CO is detected as the main product. The highest amount of CO produced over Ag-La/pCNNT is obviously higher than the amount of CO produced over the Ag-La/pCN sheets photo-catalyst. On the other hand, the highest amount of H_2 is produced over the Ag-La/pCNNT photo-catalyst compared to Ag-La/pCN sample. Similarly, Ag-La/pCNNT also promotes the amount of CH_3OH and C_2H_6. Better performance of Ag-La/pCNNT is due to 1D structure of pCNNT with more production of electrons due to nanotubes and superior separation of electrons due to protonation and Ag-La loading. These observations have been further discussed in Fig. 12(b–c). Fig. 12(b) shows the production of electrons and holes over the surface of pristine pCN sheets. The photo-generated charges would probably be recombined after their generation instead of their effective utilization in CO_2 reduction process. The fabrication of one dimensional (1D)

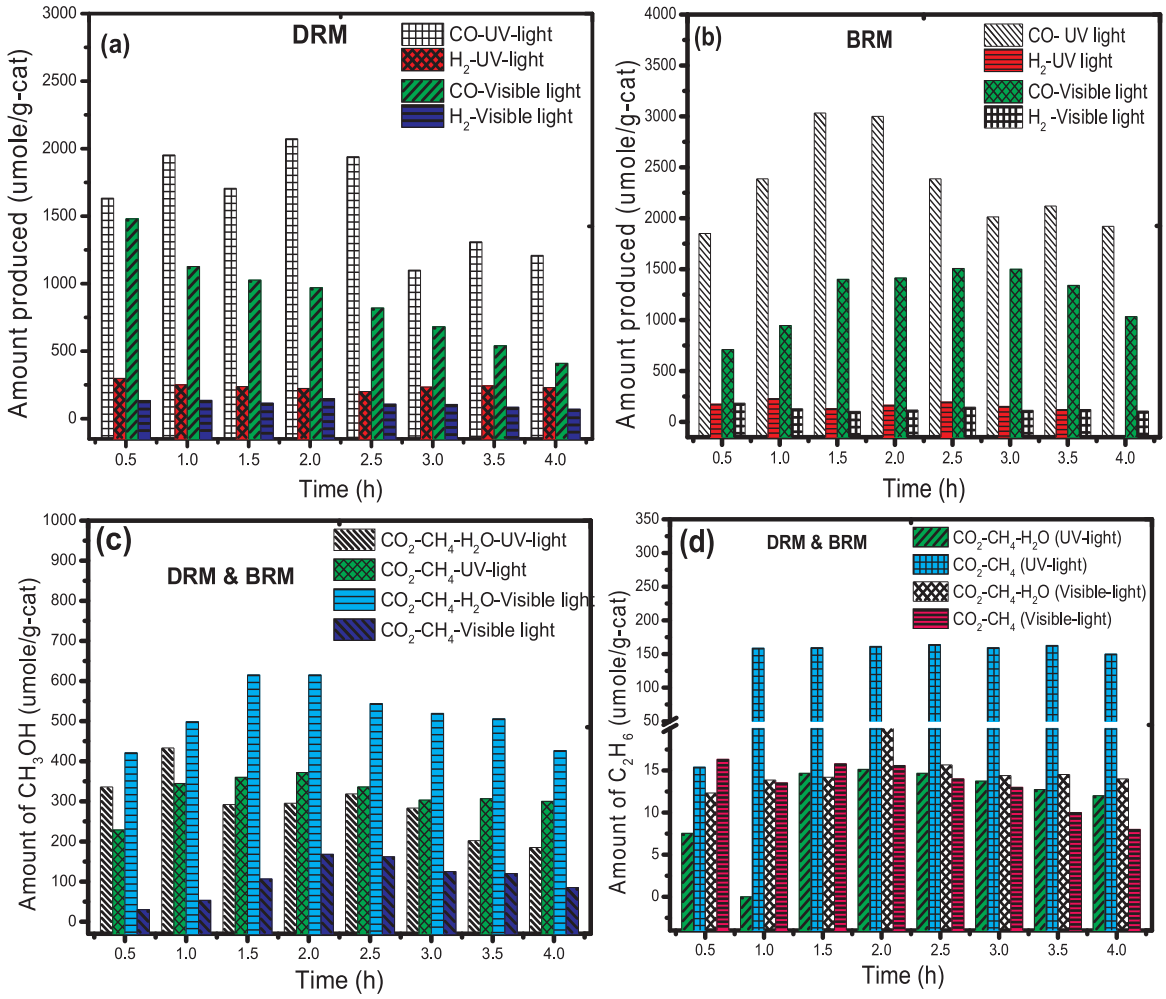

Fig. 10. Effect of type of reductants and types of light irradiation on the activity of 3% Ag-5%La-pCNNT for CO_2 reduction in a continuous fixed-bed photoreactor at 100 °C and feed flow rate 5 mL/min: (a) Dry reforming of methane for CO and H_2 production; (b) Bi-reforming of methane for CO and H_2 production; (c) CH_3OH production in dry and bi-reforming of methane; (d) C_2H_6 production in dry and bi-reforming of methane.

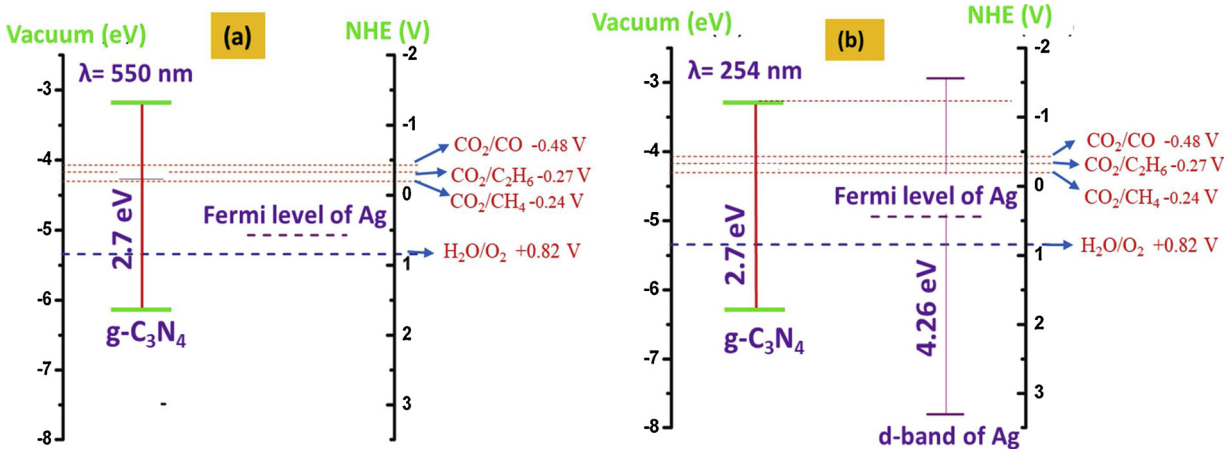

Fig. 11. Mechanism of Ag-La/pCNNT for CO_2 reduction with CH_4 in the presence of H_2O under UV and Visible light irradiations: (a) Photoactivity of Ag-La/pCNNT under visible light; (b) Photoactivity of Ag-La/pCNNT UV-light for photocatalytic bi-reforming of methane.

nanotubes would be a promising material due to faster charge separation inside pCNNT structure as presented in Fig. 12(c). Therefore, the performance of pCNNT loaded with Ag-La is attributed to more production of charges and their effective separation is due to 1D structure and hindered charges recombination rate by Ag-La.

3.2.4. Effect of reductants on Ag-La/pCNNT activity in monolithic honeycomb photoreactor

Since the type of reactor has significant contribution on the photocatalysts activity and selectivity, thus, further experiments were conducted using monolithic honeycomb photoreactor in the presence of optimized Ag-La/pCNNT photo-catalysts. For a systematic

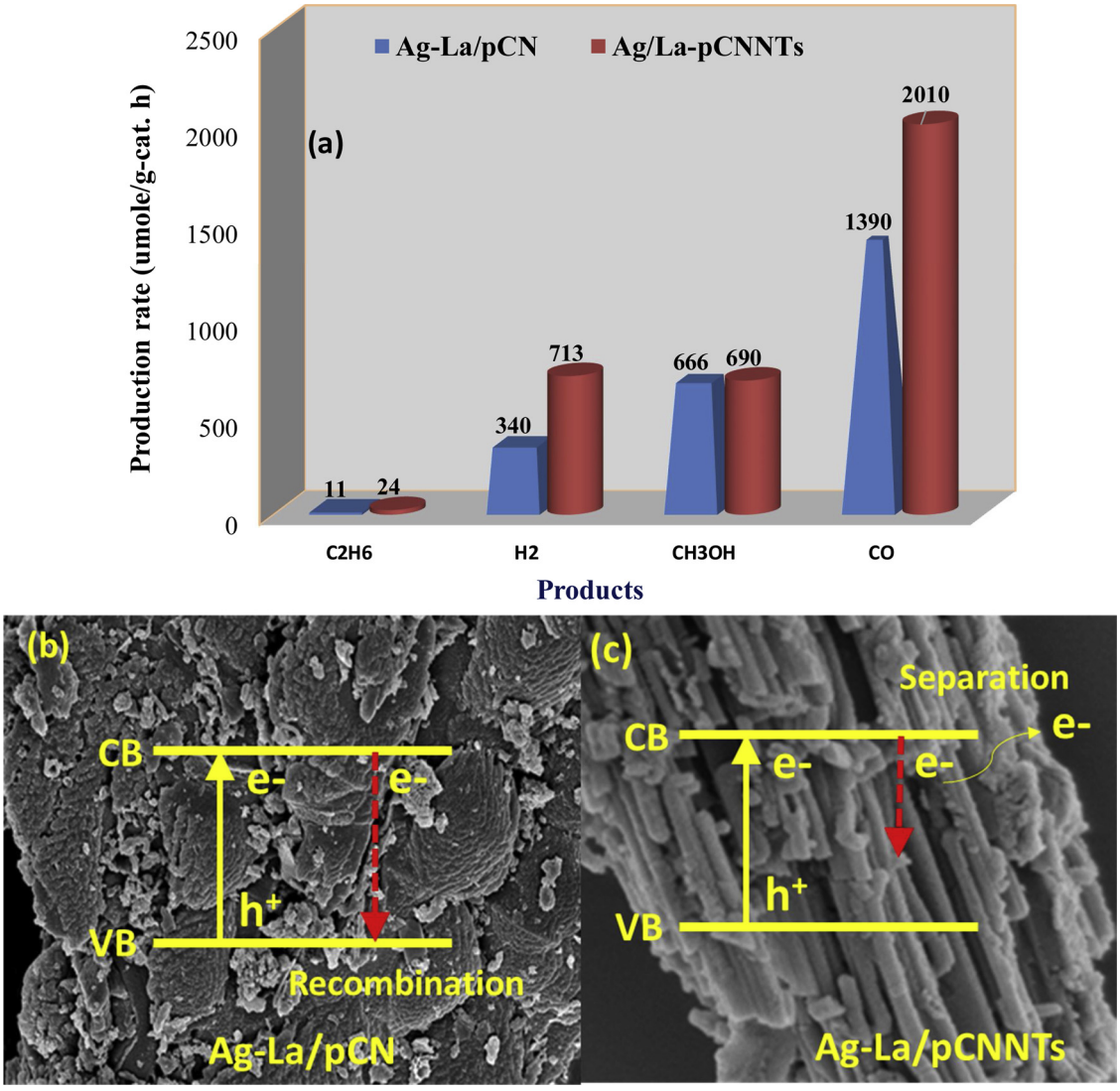

Fig. 12. (a) Effect of morphology of Ag-La/pCN and Ag-La/pCNNT for photocatalytic CO_2 reduction with CH_4 in presence of H_2O under UV-light irradiation in a fixed-bed reactor and CH_4/CO_2 feed ratio 1.0; (b) scheme of Ag-La pCN for performance analysis; (c) scheme of Ag-La pCNNT for reforming process.

understanding about the types of reforming systems, photocatalytic CO_2 reduction with H_2O, DRM and BRM processes are critically investigated. More importantly, monolith photoreactor is employed under UV-light irradiation only due to high penetration depth inside the monolith channels. Fig. 13 presents the photocatalytic CO_2 reduction using CH_4/H_2O reductants over Ag-La/pCNNT photo-catalyst for the production of CO, H_2 and CH_3OH under UV-light irradiation in a monolith photoreactor. The production of CO is lower in DRM (CO_2-CH_4) reaction system, but surge in BRM system in the presence of H_2O. At the start of reaction, production of CO is highest in all types of systems, but gradually declines over the irradiation time (Fig. 13a). This is due to adsorbed CO_2 is converted to CO and other products over irradiation time. Highest amount of CO is obtained using CO_2-CH_4-H_2O system via BRM, but no significant effect on CO production over the time on stream is observed using CO_2-CH_4 via DRM and CO_2-H_2O systems. However, the highest amount of H_2 is produced in CO_2-CH_4-H_2O via BRM reaction system compared with CO_2-CH_4 via DRM and CO_2-H_2O reactions systems as shown in Fig. 13(b). This reveals BRM reforming reactions are favourable to promote both CO and H_2 production in a monolith photoreactor. More interestingly, production of hydrocarbons is not detected in appreciable amounts, which further confirms selective BRM process for synthesis gas production. On the other hand, production of CH_3OH in Fig. 13(c) shows different trends in different reaction systems over the irradiation time. Both DRM and CO_2-H_2O systems are not favourable for CH_3OH production. Initially, the highest amount of CH_3OH is observed in BRM process, but significantly declined over time on stream. This reveals monolith reactor is not favourable for methanol and hydrocarbons production due to efficient oxidation and reduction reactions in the presence of surplus charge carriers.

The performance of fixed-bed and monolith photoreactors for photocatalytic CO_2 reduction with CH_4 via DRM and BRM is compared in Table 2. In a fixed-bed photoreactor, production rates of CO and CH_3OH for BRM is 1.46 and 3.59 folds higher than DRM under visible light irradiations. However, there is no significant effect on H_2 production rate. Under UV-light, the production rate of CO and H_2 are 2.11 and 1.41 folds higher, respectively compared to visible light irradiations during BRM in a fixed-bed reactor. Furthermore, using the monolith photoreactor, production rates of CO, H_2 and CH_3OH for BRM are 2.58, 1.99 and 2.94 folds higher, respectively compared with DRM process under UV-light irradiations. Ultimately, with BRM process under UV-light, production of H_2 and CH_3OH in a monolith photoreactor are 9.9 and 1.83 folds higher than fixed-bed reactor, while CO production is somewhat reduced.

These results could be explained based on the adsorption-desorption process with larger illuminated surface area and effective photon

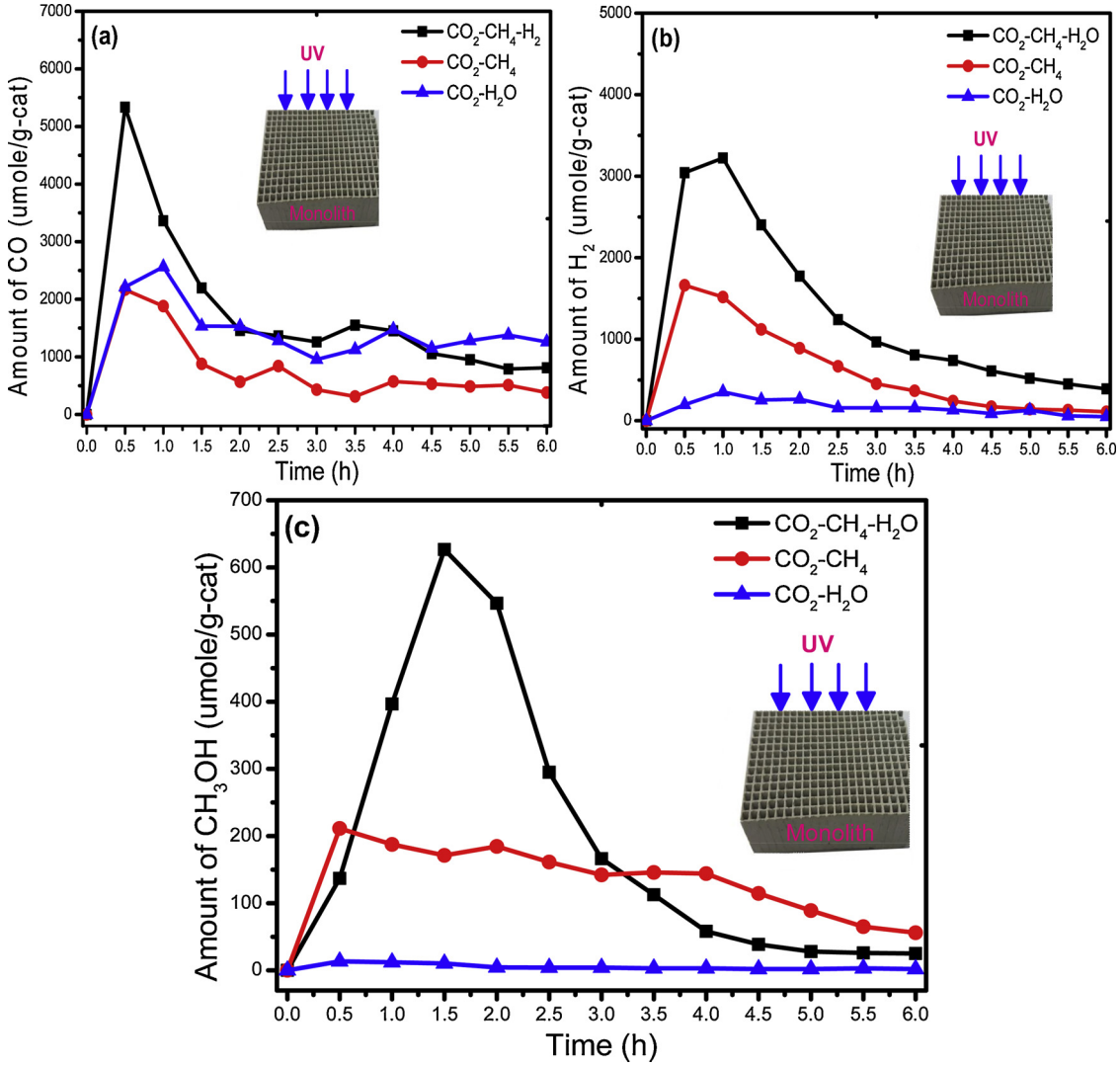

Fig. 13. Effect of reductants on the activity of 3% Ag-5% La loaded pCNNT for CO_2 reduction with CH_4/H_2O system under UV-light in a continuous monolith photoreactor: (a) CO production; (b) H_2 production; (c) CH_3OH production.

Table 2
Summary of quantum yield (%) for CO_2 reduction with different reforming processes over Ag-La-modified pCNNT catalyst.

Reductant	Type of light	Type of reactor	Production rate [a] (μmole/g-cat h)				Quantum Yield, QY [b] (%)			
			CO	H_2	CH_3OH	C_2H_6	CO	H_2	CH_3OH	C_2H_6
CO_2-CH_4	Visible light	Fixed-bed	486	79	86	8	0.299	0.049	0.053	0.0295
CO_2-CH_4-H_2O	Visible light	Fixed-bed	711	64	309	10	0.437	0.039	0.190	0.0369
CO_2-CH_4	UV-light	Fixed-bed	1038	111	186	81	0.754	0.081	0.135	0.3530
CO_2-CH_4-H_2O	UV-light	Fixed-bed	1503	90	149	12	1.092	0.065	0.108	0.0523
CO_2-H_2O	UV-light	Monolith	748	139	3	4	1.449	0.269	0.006	0.0465
CO_2-CH_4	UV-light	Monolith	298	447	93	3	0.577	0.866	0.180	0.0349
CO_2-CH_4-H_2O	UV-light	Monolith	770	891	273	5	1.492	1.726	0.527	0.0581

[a] Production rate is calculated using the equation: Production rate $= \frac{\text{Amount of specific product } (\mu mole)}{\text{weight of catalyst (g)} \times \text{time } (h)}$, weight of catalyst for fixed-bed reactor is 0.15 g, while for monolith photoreactor ~ 0.40 g ± 0.05 g.

[b] Quantum yield is calculated using Eq. (10), where n is 2, 2, 6, 14 number of electrons used for the production of CO, H_2, CH_3OH and C_2H_6 production, respectively.

energy utilization for the production of electrons in a monolith photoreactor. During DRM process, higher input energy would be required as both CO_2 and CH_4 are stable compounds. However, due to the basic nature of Ag-La modified pCNNT photo-catalyst, both CO_2 and CH_4 would be adsorbed, resulting in efficient oxidation and reduction process. Therefore, production of CO and H_2 are highest due to effective surface reactions inside the monolith photoreactor in DRM system. Furthermore, adding water to DRM would promote both CO and H_2 production owing to more protons are available. However, in a fixed-bed reactor, the products could not desorb effectively, thus higher

Table 3
Comparison of literatures on photocatalytic CO_2 reforming of CH_4 over various photo-catalysts.

Catalyst	Feed type	Reactor type	Light source	Production rate[a]	Ref.
Ag-La/pCNNT	CO_2-CH_4-H_2O	Monolith photoreactor CH_4/CO_2 ratio = 1.0 Catalyst loading~0.40 g	200 W Hg reflector lamp (150 mW/cm^2)	CO = 770 μmol h^{-1} g^{-1} H_2 = 891 μmol h^{-1} g^{-1} CH_3OH = 273 μmol h^{-1} g^{-1} C_2H_6 = 5 μmol h^{-1} g^{-1}	Current study
Ag-La/pCNNT	CO_2-CH_4-H_2O	Fixed-bed reactor Catalyst loading = 0.15 g CH_4/CO_2 ratio = 1.0 Temperature = 100 °C	200 W Hg reflector lamp (150 mW/cm^2)	CO = 1503 μmol h^{-1} g^{-1} H_2 = 90 μmol h^{-1} g^{-1} CH_3OH = 149 C_2H_6 = 10 μmol h^{-1} g^{-1}	Current study
Ag-La/pCNNT	CO_2-CH_4-H_2O	Fixed-bed reactor Catalyst loading = 0.15 g CH_4/CO_2 ratio = 1.0 Temperature = 100 °C	LCS 100, Solar simulator (100 mW/cm^2)	CO = 711 μmol h^{-1} g^{-1} H_2 = 64 μmol h^{-1} g^{-1} CH_3OH = 309 μmol h^{-1} g^{-1} C_2H_6= μmol h^{-1} g^{-1}	Current study
La/TiO_2	CO_2-CH_4	Fixed-bed reactor Catalyst loading = 0.15 g CH_4/CO_2 ratio = 1.0 Temperature = 100 °C	200 W Hg lamp (150 mW/cm^2)	CO = 183 μmol h^{-1} g^{-1} H_2 = 74 μmol h^{-1} g^{-1} C_2H_6 = 172 μmol h^{-1} g^{-1}	[55]
Cu/g-C_3N_4	CO_2-CH_4	Fixed-bed reactor, Catalyst = 0.15 g CH_4/CO_2 ratio = 1.0	LCS 100, Solar simulator (100 mW/cm^2)	CO = 142 μmol h^{-1} g^{-1} H_2 = 76 μmol h^{-1} g^{-1} C_2H_6 = 2.0 μmol h^{-1} g^{-1}	[56]
Au/TNTs	CO_2-CH_4	Quartz fixed-bed reactor, Catalyst = 0.50 g,	500 W lamp 0.14 W/m^2, (190-350 nm)	CO = 11.9 μmol h^{-1} g^{-1} H_2 = 104 μmol h^{-1} g^{-1} C_2H_6 = 11.4 μmol h^{-1} g^{-1} CH_3OH = 0.95 μmol h^{-1} g^{-1}	[54]
Ga_2O_3	CO_2-CH_4	Quartz fixed-bed reactor Temp = 673 K Catalyst = 0.20 g	300 W Xe- Lamp, 9 mW/cm^2 (220-330 nm)	CO = 3.82 μmol h^{-1} g^{-1} H_2 = 10.53 μmol h^{-1} g^{-1} C_2H_6 = 1.2 μmol h^{-1} g^{-1}	[53]
MgO	CO_2-CH_4	Fixd-bed reactor Dead space = 18.9 mL, Catalyst = 0.30 g	500-W Hg lamp	CO = 3.6 μmole H_2 = 0.05 μmole	[52]

production rate of CO was obtained, resulting in a lower H_2/CO ratio. Similarly, monolith photoreactor has limitations under visible light irradiations due to microchannel and light could not pass through the channels due to lower penetration depth compared to fixed-bed reactor. Therefore, monolithic honeycomb photoreactor and BRM reaction system promoted both CO and H_2 production under UV-light irradiations due to higher photon energy utilization with efficient desorption process and minimum mass transfer limitations.

3.2.5. Quantum yield and performance analysis

The ideal approach to compare the performance of different reactors operating under different types of light irradiations with different photon flux by measuring the quantum yield (QY). It is also important to evaluate the photo-catalysts performance by considering the amounts of energy consumed and rate of products under the same process conditions. Herein, photocatalytic quantum yield (%) for producing CO, H_2 C_2H_6 and CH_3OH has been calculated using Eq. (10).

$$\text{Quantum Yield,} \quad QY\ (\%) = \frac{n \times production\ rate\ (\mu mole/s)}{photon\ flux\ (\mu mole/\ s)} \tag{10}$$

where n is the number of electrons used for CO, H_2, CH_3OH and C_2H_6 production, which are 2, 2, 6 and 14 electrons, respectively. The QY is calculated using UV-light intensity of 150 mW cm^{-2}, λ = 254 nm; for visible light, solar light intensity of 100 mW cm^{-2} and λ = 450 nm has been employed. The results for different reforming systems, types of light irradiations and reactor types are presented in Table 2. Evidently, the highest QY is obtained for BRM reaction system for CO and H_2 production in a monolith photoreactor system. By comparing the source of light irradiations, it is obvious that UV-light provides more energy to break both CO_2 and CH_4 stable molecules compared to visible light irradiations. The QY during photocatalytic BRM process for CO production in a monolith photo-reactor is 1.4 folds higher than fixed-bed reactor. More interestingly, QY for H_2 evolution BRM process is 26.6 folds higher in a monolith photoreactor compared to fixed- bed reactor under UV-light irradiations. Similar trends as the fixed-bed reactor is observed in the performance of the monolith photoreactor in DRM process for CO and H_2 production. In addition, the monolith during photoreactor has more potential for significantly improving H_2 production in all types of reforming systems. More importantly, QY of 0.527% for methanol is obtained in the monolith photoreactor, 4.9 folds higher than using fixed- bed reactor under UV-light irradiations. Thus, even with the same active sites and photon flux, production rate would be different due to different utilization of photon energy with different production of electrons and behaviour of adsorption competitions in different types of photo-reactors. The significantly enhanced performance of monolith photoreactor is obviously due to more photon flux utilization inside the monolith photoreactor compared to fixed-bed reactor, resulting in significantly improved productivity. This reveals that in BRM all reactants i.e., CO_2, CH_4 and H_2O are adsorbed over the catalyst surface in the monolith photoreactor and effectively converted to products due to more production of electrons with improved utilization of incident photon flux. The hydrogen enriched syngas could be obtained by combining DRM and SRM process as similarly reported in thermal reforming process [49].

Previously, Liou et al. [50], reported photo-catalytic CO_2 reduction with H_2O in an internally illuminated monolith photoreactor with NiO/$InTaO_4$ photo-catalyst and quantum efficiency of 0.012% for methanol production was obtained under visible light, while a quantum efficiency of 0.057% was observed for acetaldehyde under UV-light irradiations. Similarly, Ru-Pd/TiO_2 catalyst was employed for photocatalytic CO_2 reduction with H_2O in an internally illuminated monolith photoreactor with QY of 0.015% for CH_4. Using the same catalyst in a slurry photoreactor, 0.002% QY was obtained for CH_4 production under UV-light irradiations [51]. Although, in previous works monolith reactor was employed with optical fibre to increase illumination inside monolith channels, QY was relatively low. A significant improvement in QY in the current study is attributed to bimetallic Ag-La loaded pCNNT over the monolithic channels. Photon energy is efficiently utilized during photocatalytic BRM reactions for selective CO and H_2 evolutions.

The performance of Ag-La modified pCNNT was further compared with the results of previous researchers employed for photocatalytic CO_2 reduction with CH_4 as summarized in Table 3. MgO was used for photocatalytic CO_2 reduction with CH_4 and products obtained were CO (3.6 μmole) and H_2 (0.5 μmole) under UV-light irradiations [52].

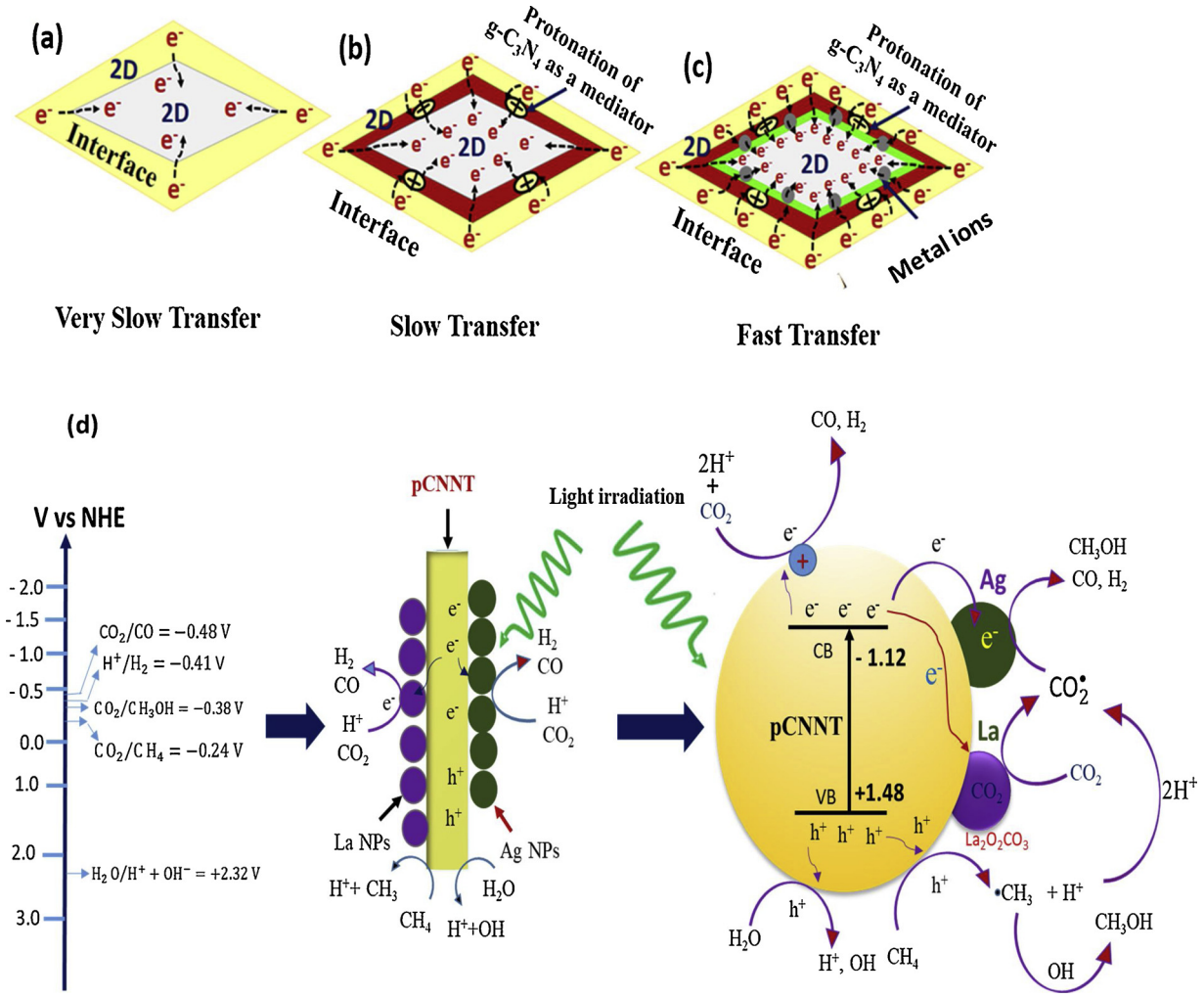

Fig. 14. Schematic presentation of synergistic effects of Ag-La loaded pCNNT for photocatalytic CO_2-CH_4 conversion in presence of H_2O.

Similarly, Ga_2O_3 was tested for photocatalytic CO_2 reduction with CH_4 in a fixed-bed reactor at temperature of 673 K [53]. The products obtained were CO, H_2 and C_2H_6 with production rate of 3.82, 10.53, and 1.2 μmole g-cat^{-1} h^{-1}, respectively under UV-light irradiation. Another work, Au/TNTs was investigated for photocatalytic CO_2 reduction by CH_4 under UV-light irradiations and the products obtained were CO, H_2, C_2H_6 and CH_3OH with their production rate 11.9, 104, 11.4 and 0.95 μmole g-cat^{-1} h^{-1}, respectively [54]. Recently, we reported photocatalytic CO_2 reduction with CH_4 under UV-light irradiation in a fixed-bed photoreactor at 373 K. The products observed were CO, H_2 and C_2H_6 with production rate 183, 74, and 172 μmole g-cat^{-1} h^{-1}, respectively [55]. By comparing all the results with the current study, it is evident that production rates of CO and H_2 during photocatalytic bireforming of methane were much higher over Ag-La/pCNNT in a monolith photoreactor. Thus, the efficiency and selectivity of synthesis gas production can be improved for photocatalytic CO_2 reduction with CH_4 in the presence of H_2O in a monolith photoreactor. In general, better performance was due to larger irradiated surface area, higher quantum flux and improved sorption process.

3.3. Reaction mechanism of photo-induced CO_2 reduction with CH_4/H_2O

In order to understand the enhanced performance of Ag-La loaded pCNNT and multi-step electron process for the production of CO, H_2, CH_3OH and C_2H_6 during photocatalytic CO_2 reduction with CH_4/H_2O, following reaction mechanism can be established as explained in Eqs. (11)–(21) [28,57].

$$CN \rightarrow e^- + h^+ \quad (11)$$

$$La^{3+} + 3e^- \rightarrow La \quad (12)$$

$$Ag^{2+} + 2e^- \rightarrow Ag \quad (13)$$

$$CO_2 + e^- \rightarrow CO_2^{\bullet -} \quad (14)$$

$$H_2O + h^+ \rightarrow OH^{\bullet} + H^+ \quad (15)$$

$$CH_4 + OH^{\bullet} \rightarrow H_2O + CH_3^{\bullet} \quad (16)$$

$$CH_4 + h^+ \rightarrow CH_3^{\bullet} + H^+ \quad (17)$$

$$CO_2^{\bullet -} + 2H^+ + e^- \rightarrow CO + H_2O \quad (18)$$

$$CH_3^{\bullet} + CH_3^{\bullet} \rightarrow C_2H^6 \quad (19)$$

$$2H^+ + 2e^- \rightarrow H_2 \quad (20)$$

$$CH_3^{\bullet} + OH^{\bullet} \rightarrow CH_3OH \quad (21)$$

In the first step, charge carriers are produced over pCNNT surface by the strike of UV and visible light irradiations. Electrons are readily transferred towards Ag-La on the surface of pCNNT for the reduction of CO_2 as discussed in Eqs. (11)–(14). In the second step, CH_4 and H_2O were oxidized by the holes and hydroxyl ions (OH^-) through the reactions in Eqs. (15)–(17). Finally, production of CO, C_2H_6 and H_2 were obtained through the reactions in Eqs. (18)–(20). The production of CH_3OH was obtained through CH_3 radicals and hydroxyl ions reaction by Eq. (21). In addition, La_2O_3 also contributes in the cleavage of C—H

bonds in CH_4, resulting in enhanced CH_3 and H^+ evolution. Therefore, Ag is favourable for enhanced CO_2 reduction while La promoted CH_4 oxidation, and this effectively enhanced photocatalytic activity toward CO, H_2 and CH_3OH production.

The possible schematic for photocatalytic bi-reforming of methane towards CO, C_2H_6, CH_3OH and H_2 compounds over pCNNT due to the combined effect of Ag and La is depicted in Fig. 14. The embedded Ag over the surface of pCNNT by the process of UV photo-deposition has strong interaction between pCNNT and La_2O_3, which is profitable for dynamic separation of photo-generated electrons and holes toward CO_2 for its reduction. Furthermore, band gap energy of pCNNT is ~2.60 eV which is suitable for both UV and visible light irradiations for its activation. In addition, production of CO, H_2, CH_3OH and C_2H_6 could be explained based on their reduction potentials. For example, conductance band of pCNNT (−1.12 V) is more negative than the reduction potential of CO_2/CO, CO_2/CH_3OH (−0.38 V), H^+/H_2 (−0.41 V) and CO_2/C_2H_6 (−0.26 V). Thus, these products are thermodynamically favourable. Furthermore, C_2H_6 could be produced through multistep process which involves CH_4 oxidation and coupling of CH_3 radicals. When H_2O was added to CO_2-CH_4 reaction system, H^+ and OH would be produced. The H^+ could be converted to H_2 or consumed by CO_2 for the generation of CO. Besides, OH radicals produced during H_2O oxidation can promote oxidation of CH_4 to produce CH_3 radicals and H^+ ions, and finally the production of C_2H_6 and H_2. Using monolithic support, there would be a larger photon energy utilization, with effective transport of electrons/holes and desorption of production, resulting in greater photocatalytic activity. Therefore, it is demonstrated that synergistic effect of Ag-La is favourable for improved CO_2 reduction and CH_4 oxidation towards proficient production of CO, H_2 and CH_3OH, while efficiency can further be enhanced using CO_2-CH_4-H_2O reaction system and monolithic support.

4. Conclusions

Ag-La-loaded pCNNT samples are successfully synthesized using hydrothermal and sonication methods. Introducing Ag promotes separation of electrons, while La is favourable for controlling basicity and cleavage of CH_4, enhancing oxidation and reduction processes. However, significantly enhanced photo-activity is mainly attributed to Ag-La loaded pCNNT with controlled morphology and adsorption-desorption process with faster charge carrier separation. Using DRM system, CO, H_2 and C_2H_6 are produced in significant amounts, while BRM promoted the production of CO and H_2 under the same process conditions. Compared to visible light, the performance of composite catalyst under UV light irradiation is more efficient due to its stronger penetration power and more intensity to break stable CO_2 and CH_4 molecules. The QY during photocatalytic BRM process for CO production in a monolith photo-reactor is 1.4 folds higher than fixed-bed reactor. More interestingly, QY for H_2 evolution during BRM process is 26.6 folds higher in a monolith photoreactor compared to fixed-bed reactor under UV-light irradiations. Therefore, using UV-light irradiations and monolithic honeycomb support the performance of Ag-La-loaded pCNNT can be maximized for dynamic BRM to selective fuels. The results of this study contribute to the development of new advanced hetero-structures using facile method for CO_2 conversion applications in the monolithic photoreactor under UV-light irradiations.

Acknowledgements

The authors would like to express their since gratitude for the financial support of this work under Nanomite Long Term Research Grant Scheme (LRGS) Vot 4L839 and MRSA-FRGS Vot 4F988 from the Ministry of Education (MOE), Malaysia and project 03-01-06-SF1437, Vot 4S133 from the Ministry of Energy, Science, Technology, Environment and Climate Change, (MESTECC), Malaysia.

References

[1] A. Olivo, V. Trevisan, E. Ghedini, F. Pinna, C.L. Bianchi, A. Naldoni, G. Cruciani, M. Signoretto, CO_2photoreduction with water: catalyst and process investigation, J. CO_2 Util. 12 (2015) 86–94, https://doi.org/10.1016/j.jcou.2015.06.001.
[2] X. Chang, T. Wang, J. Gong, CO_2 photo-reduction: insights into CO_2 activation and reaction on surfaces of photocatalysts, Energy Environ. Sci. 9 (2016) 2177–2196, https://doi.org/10.1039/c6ee00383d.
[3] H. Abdullah, M.M.R. Khan, H.R. Ong, Z. Yaakob, Modified TiO_2 photocatalyst for CO_2photocatalytic reduction: an overview, J. CO_2 Util. 22 (2017) 15–32, https://doi.org/10.1016/j.jcou.2017.08.004.
[4] Y. Sohn, W. Huang, F. Taghipour, Recent progress and perspectives in the photocatalytic CO_2 reduction of Ti-oxide-based nanomaterials, Appl. Surf. Sci. 396 (2017) 1696–1711, https://doi.org/10.1016/j.apsusc.2016.11.240.
[5] J.Y. Do, Y. Im, B.S. Kwak, J.-Y. Kim, M. Kang, Dramatic CO_2 photoreduction with H_2O vapors for CH_4 production using the TiO_2 (bottom)/Fe–TiO_2 (top) double-layered films, Chem. Eng. J. 275 (2015) 288–297, https://doi.org/10.1016/j.cej.2015.03.066.
[6] Y. Wang, F. Wang, Y. Chen, D. Zhang, B. Li, S. Kang, X. Li, L. Cui, Enhanced photocatalytic performance of ordered mesoporous Fe-doped CeO_2 catalysts for the reduction of CO_2 with H_2O under simulated solar irradiation, Appl. Catal. B: Environ. 147 (2014) 602–609, https://doi.org/10.1016/j.apcatb.2013.09.036.
[7] Z. Zhu, J. Qin, M. Jiang, Z. Ding, Y. Hou, Enhanced selective photocatalytic CO_2 reduction into CO over Ag/CdS nanocomposites under visible light, Appl. Surf. Sci. 391 (2017) 572–579, https://doi.org/10.1016/j.apsusc.2016.06.148.
[8] E. Karamian, S. Sharifnia, On the general mechanism of photocatalytic reduction of CO_2, J. CO_2 Util. 16 (2016) 194–203, https://doi.org/10.1016/j.jcou.2016.07.004.
[9] Z. Xiong, Y. Zhao, J. Zhang, C. Zheng, Efficient photocatalytic reduction of CO_2 into liquid products over cerium doped titania nanoparticles synthesized by a sol–gel auto-ignited method, Fuel Process. Technol. 135 (2015) 6–13, https://doi.org/10.1016/j.fuproc.2014.09.017.
[10] D.O. Adekoya, M. Tahir, N.A.S. Amin, g-C_3N_4/(Cu/TiO_2) nanocomposite for enhanced photoreduction of CO_2 to CH_3OH and HCOOH under UV/visible light, J. CO_2 Util. 18 (2017) 261–274, https://doi.org/10.1016/j.jcou.2017.02.004.
[11] L. Xu, F. Wang, M. Chen, X. Fan, H. Yang, D. Nie, L. Qi, Alkaline-promoted Co-Ni bimetal ordered mesoporous catalysts with enhanced coke-resistant performance toward CO_2 reforming of CH_4, J. CO_2 Util. 18 (2017) 1–14, https://doi.org/10.1016/j.jcou.2017.01.003.
[12] A.H. Khoja, M. Tahir, N.A.S. Amin, Dry reforming of methane using different dielectric materials and DBD plasma reactor configurations, Energy Convers. Manage. 144 (2017) 262–274, https://doi.org/10.1016/j.enconman.2017.04.057.
[13] A. Moral, I. Reyero, C. Alfaro, F. Bimbela, L.M. Gandia, Syngas production by means of biogas catalytic partial oxidation and dry reforming using Rh-based catalysts, Catal. Today 299 (2018) 280–288, https://doi.org/10.1016/j.cattod.2017.03.049.
[14] J. Goscianska, R. Pietrzak, J. Matos, Catalytic performance of ordered mesoporous carbons modified with lanthanides in dry methane reforming, Catal. Today 301 (2018) 204–216, https://doi.org/10.1016/j.cattod.2017.05.014.
[15] R. Dębek, M. Motak, M.E. Galvez, T. Grzybek, P. Da Costa, Promotion effect of zirconia on Mg(Ni,Al)O mixed oxides derived from hydrotalcites in CO_2 methane reforming, Appl. Catal. B: Environ. 223 (2018) 36–46, https://doi.org/10.1016/j.apcatb.2017.06.024.
[16] D. Shi, Y. Feng, S. Zhong, Photocatalytic conversion of CH_4 and CO_2 to oxygenated compounds over Cu/CdS-TiO_2/SiO_2 catalyst, Catal. Today 98 (2004) 505–509, https://doi.org/10.1016/j.cattod.2004.09.004.
[17] K. Teramura, T. Tanaka, H. Ishikawa, Y. Kohno, T. Funabiki, Photocatalytic reduction of CO_2 to CO in the presence of H_2 or CH_4 as a reductant over MgO, J. Phys. Chem. B 108 (2004) 346–354.
[18] B. Han, W. Wei, L. Chang, P. Cheng, Y.H. Hu, Efficient visible light photocatalytic CO_2 reforming of CH_4, ACS Catal. 6 (2015) 494–497, https://doi.org/10.1021/acscatal.5b02653.
[19] T. Stroud, T.J. Smith, E. Le Saché, J.L. Santos, M.A. Centeno, H. Arellano-Garcia, J.A. Odriozola, T.R. Reina, Chemical CO_2 recycling via dry and bi reforming of methane using Ni-Sn/Al_2O_3 and Ni-Sn/CeO_2-Al_2O_3 catalysts, Appl. Catal. B: Environ. 224 (2018) 125–135, https://doi.org/10.1016/j.apcatb.2017.10.047.
[20] S.S. Itkulova, Y.Y. Nurmakanov, S.K. Kussanova, Y.A. Boleubayev, Production of a hydrogen-enriched syngas by combined CO_2-steam reforming of methane over Co-based catalysts supported on alumina modified with zirconia, Catal. Today 299 (2018) 272–279, https://doi.org/10.1016/j.cattod.2017.07.014.
[21] E.H. Yang, Y.S. Noh, G.H. Hong, D.J. Moon, Combined steam and CO_2 reforming of methane over La1-xSrxNiO_3 perovskite oxides, Catal. Today 299 (2018) 242–250, https://doi.org/10.1016/j.cattod.2017.03.050.
[22] H. Gao, P. Zhang, J. Zhao, Y. Zhang, J. Hu, G. Shao, Plasmon enhancement on photocatalytic hydrogen production over the Z-scheme photosynthetic heterojunction system, Appl. Catal. B: Environ. 210 (2017) 297–305, https://doi.org/10.1016/j.apcatb.2017.03.050.
[23] X. Hao, J. Zhou, Z. Cui, Y. Wang, Y. Wang, Z. Zou, Zn-vacancy mediated electron-hole separation in ZnS/g-C_3N_4 heterojunction for efficient visible-light photocatalytic hydrogen production, Appl. Catal. B: Environ. 229 (2018) 41–51, https://doi.org/10.1016/j.apcatb.2018.02.006.
[24] M. Li, L. Zhang, M. Wu, Y. Du, X. Fan, M. Wang, L. Zhang, Q. Kong, J. Shi, Mesostructured CeO_2/g-C_3N_4 nanocomposites: remarkably enhanced photocatalytic activity for CO_2 reduction by mutual component activations, Nano Energy 19 (2016) 145–155, https://doi.org/10.1016/j.nanoen.2015.11.010.
[25] K.P. Priyanka, V.R. Revathy, P. Rosmin, B. Thrivedu, K.M. Elsa, J. Nimmymol, K.M. Balakrishna, T. Varghese, Influence of La doping on structural and optical

properties of TiO2 nanocrystals, Mater. Charact. 113 (2016) 144–151, https://doi.org/10.1016/j.matchar.2016.01.015.
[26] L. Yu, X. Yang, J. He, Y. He, D. Wang, One-step hydrothermal method to prepare nitrogen and lanthanum co-doped TiO_2 nanocrystals with exposed {001} facets and study on their photocatalytic activities in visible light, J. Alloys Compd. 637 (2015) 308–314, https://doi.org/10.1016/j.jallcom.2015.03.035.
[27] S.J. Armaković, M. Grujić-Brojčin, M. Šćepanović, S. Armaković, A. Golubović, B. Babić, B.F. Abramović, Efficiency of La-doped TiO_2 calcined at different temperatures in photocatalytic degradation of β-blockers, Arabian J. Chem. (2017), https://doi.org/10.1016/j.arabjc.2017.01.001.
[28] Y. Liu, S. Zhou, J.M. Li, Y.J. Wang, G.Y. Jiang, Z. Zhao, B. Liu, X.Q. Gong, A.J. Duan, J. Liu, Y.C. Wei, L.Q. Zhang, Photocatalytic reduction of CO_2 with water vapor on surface La-modified TiO_2 nanoparticles with enhanced CH_4 selectivity, Appl. Catal. B: Environ. 168 (2015) 125–131, https://doi.org/10.1016/j.apcatb.2014.12.011.
[29] B. Tahir, M. Tahir, N.A.S. Amin, Photocatalytic carbon dioxide and methane reduction to fuels over La-promoted titanium dioxide nanocatalyst, Chem. Eng. Trans. 56 (2017) 1123–1128, https://doi.org/10.3303/CET1756188.
[30] D. Xu, B. Cheng, W. Wang, C. Jiang, J. Yu, Ag_2CrO_4/g-C_3N_4 /graphene oxide ternary nanocomposite Z-scheme photocatalyst with enhanced CO_2 reduction activity, Appl. Catal. B: Environ. 242 (2018) 139–147, https://doi.org/10.1016/j.apcatb.2018.03.036.
[31] M. Tahir, B. Tahir, N.A.S. Amin, Z.Y. Zakaria, Photo-induced reduction of $CO_2$to CO with hydrogen over plasmonic Ag-NPs/TiO 2 NWs core/shell hetero-junction under UV and visible light, J. CO_2 Util. 18 (2017) 250–260, https://doi.org/10.1016/j.jcou.2017.02.002.
[32] J. Qin, H. Zeng, Photocatalysts fabricated by depositing plasmonic Ag nanoparticles on carbon quantum dots/graphitic carbon nitride for broad spectrum photocatalytic hydrogen generation, Appl. Catal. B: Environ. 209 (2017) 161–173, https://doi.org/10.1016/j.apcatb.2017.03.005.
[33] M. Tahir, B. Tahir, N.A.S. Amin, Synergistic effect in plasmonic Au/Ag alloy NPs co-coated TiO_2 NWs toward visible-light enhanced CO_2 photoreduction to fuels, Appl. Catal. B: Environ. 204 (2017) 548–560, https://doi.org/10.1016/j.apcatb.2016.11.062.
[34] M. Tahir, N.A.S. Amin, Photo-induced CO_2 reduction by hydrogen for selective CO evolution in a dynamic monolith photoreactor loaded with Ag-modified TiO_2 nanocatalyst, Int. J. Hydrogen Energy 42 (2017) 15507–15522, https://doi.org/10.1016/j.ijhydene.2017.05.039.
[35] Q. Lang, Y. Chen, T. Huang, L. Yang, S. Zhong, L. Wu, J. Chen, S. Bai, Graphene "bridge" in transferring hot electrons from plasmonic Ag nanocubes to TiO_2 nanosheets for enhanced visible light photocatalytic hydrogen evolution, Appl. Catal. B: Environ. 220 (2018) 182–190, https://doi.org/10.1016/j.apcatb.2017.08.045.
[36] J. Low, S. Qiu, D. Xu, C. Jiang, B. Cheng, Direct evidence and enhancement of surface plasmon resonance effect on Ag-loaded TiO_2 nanotube arrays for photocatalytic CO_2 reduction, Appl. Surf. Sci. 434 (2018) 423–432, https://doi.org/10.1016/j.apsusc.2017.10.194.
[37] H. Li, Y. Gao, X. Wu, P.-H. Lee, K. Shih, Fabrication of heterostructured g-C_3N_4/Ag-TiO_2 hybrid photocatalyst with enhanced performance in photocatalytic conversion of CO_2 under simulated sunlight irradiation, Appl. Surf. Sci. 402 (2017) 198–207, https://doi.org/10.1016/j.apsusc.2017.01.041.
[38] A. Bafaqeer, M. Tahir, N.A.S. Amin, Well-designed ZnV_2O_6/g-C_3N_4 2D/2D nanosheets heterojunction with faster charges separation via pCN as mediator towards enhanced photocatalytic reduction of CO_2 to fuels, Appl. Catal. B: Environ. 242 (2019) 312–326, https://doi.org/10.1016/j.apcatb.2018.09.097.
[39] Z. Guan, Z. Xu, Q. Li, P. Wang, G. Li, J. Yang, AgIn 5 S 8 nanoparticles anchored on 2D layered ZnIn 2 S 4 to form 0D/2D heterojunction for enhanced visible-light photocatalytic hydrogen evolution, Appl. Catal. B: Environ. 227 (2018) 512–518, https://doi.org/10.1016/j.apcatb.2018.01.068.
[40] B. Lin, H. Li, H. An, W. Hao, J. Wei, Y. Dai, C. Ma, G. Yang, Preparation of 2D/2D g-C_3N_4 nanosheet@$ZnIn_2S_4$ nanoleaf heterojunctions with well-designed high-speed charge transfer nanochannels towards high-efficiency photocatalytic hydrogen evolution, Appl. Catal. B: Environ. 220 (2018) 542–552, https://doi.org/10.1016/j.apcatb.2017.08.071.
[41] W. Feng, Y. Wang, X. Huang, K. Wang, F. Gao, Y. Zhao, B. Wang, L. Zhang, P. Liu, One-pot construction of 1D/2D Zn_{1-x} Cd_xS/D-$ZnS_{(en)0.5}$ composites with perfect heterojunctions and their superior visible-light-driven photocatalytic H_2 evolution, Appl. Catal. B: Environ. 220 (2018) 324–336, https://doi.org/10.1016/j.apcatb.2017.08.002.
[42] Z. Xiong, Z. Lei, S. Ma, X. Chen, B. Gong, Y. Zhao, J. Zhang, C. Zheng, J.C.S. Wu, Photocatalytic CO_2 reduction over v and W codoped TiO_2 catalyst in an internal-illuminated honeycomb photoreactor under simulated sunlight irradiation, Appl. Catal. B: Environ. 219 (2017) 412–424, https://doi.org/10.1016/j.apcatb.2017.07.078.
[43] B. Tahir, M. Tahir, N.S. Amin, Performance analysis of monolith photoreactor for CO_2 reduction with H_2, Energy Convers. Manage. 90 (2015) 272–281, https://doi.org/10.1016/j.enconman.2014.11.018.
[44] L. Muniandy, F. Adam, A.R. Mohamed, A. Iqbal, N.R.A. Rahman, Cu^{2+} coordinated graphitic carbon nitride (Cu-g-C_3N_4) nanosheets from melamine for the liquid phase hydroxylation of benzene and VOCs, Appl. Surf. Sci. 398 (2017) 43–55, https://doi.org/10.1016/j.apsusc.2016.11.103.
[45] J. Jiang, J. Yu, S. Cao, Au/PtO nanoparticle-modified g-C_3N_4 for plasmon-enhanced photocatalytic hydrogen evolution under visible light, J. Colloid Interface Sci. 461 (2016) 56–63, https://doi.org/10.1016/j.jcis.2015.08.076.
[46] X. Xu, Z. Si, L. Liu, Z. Wang, Z. Chen, R. Ran, Y. He, D. Weng, $CoMoS_2$ /rGO/C 3 N 4 ternary heterojunctions catalysts with high photocatalytic activity and stability for hydrogen evolution under visible light irradiation, Appl. Surf. Sci. 435 (2018) 1296–1306, https://doi.org/10.1016/j.apsusc.2017.12.001.
[47] M. Wu, M. Zhang, T. Lv, M. Guo, J. Li, C.A. Okonkwo, Q. Liu, L. Jia, The effect of calcination atmosphere upon the photocatalytic performance of Au-La_2O_3/TiO_2 for hydrogen production from formic acid, Appl. Catal. A: Gen. 547 (2017) 96–104, https://doi.org/10.1016/j.apcata.2017.08.027.
[48] C. Zhang, Y. Zhou, J. Bao, J. Fang, S. Zhao, Y. Zhang, X. Sheng, W. Chen, Structure regulation of ZnS@g-C_3N_4/TiO_2 nanospheres for efficient photocatalytic H_2 production under visible-light irradiation, Chem. Eng. J. 346 (2018) 226–237, https://doi.org/10.1016/j.cej.2018.04.038.
[49] S.S. Itkulova, Y.Y. Nurmakanov, S.K. Kussanova, Y.A. Boleubayev, Production of a hydrogen-enriched syngas by combined CO_2 -steam reforming of methane over Co-based catalysts supported on alumina modified with zirconia, Catal. Today 299 (2018) 272–279, https://doi.org/10.1016/j.cattod.2017.07.014.
[50] P.-Y. Liou, S.-C. Chen, J.C.S. Wu, D. Liu, S. Mackintosh, M. Maroto-Valer, R. Linforth, Photocatalytic CO_2 reduction using an internally illuminated monolith photoreactor, Energy Environ. Sci. 4 (2011) 1487, https://doi.org/10.1039/c0ee00609b.
[51] O. Ola, M. Maroto-Valer, D. Liu, S. Mackintosh, C.-W. Lee, J.C.S. Wu, Performance comparison of CO_2 conversion in slurry and monolith photoreactors using Pd and Rh-TiO_2 catalyst under ultraviolet irradiation, Appl. Catal. B: Environ. 126 (2012) 172–179, https://doi.org/10.1016/j.apcatb.2012.07.024.
[52] K. Teramura, T. Tanaka, H. Ishikawa, Y. Kohno, T. Funabiki, Photocatalytic reduction of CO_2 to CO in the presence of H_2 or CH_4 as a reductant over MgO, J. Phys. Chem. B 108 (2004) 346–354, https://doi.org/10.1021/jp0362943.
[53] L. Yuliati, H. Itoh, H. Yoshida, Photocatalytic conversion of methane and carbon dioxide over gallium oxide, Chem. Phys. Lett. 452 (2008) 178–182.
[54] B. László, K. Baán, E. Varga, A. Oszkó, A. Erdőhelyi, Z. Kónya, J. Kiss, Photo-induced reactions in the CO_2-methane system on titanate nanotubes modified with Au and Rh nanoparticles, Appl. Catal. B: Environ. 199 (2016) 473–484, https://doi.org/10.1016/j.apcatb.2016.06.057.
[55] B. Tahir, M. Tahir, N.A.S. Amin, Tailoring performance of La-modified TiO_2 nanocatalyst for continuous photocatalytic CO_2 reforming of CH_4 to fuels in the presence of H_2O, Energy Convers. Manage. 159 (2018) 284–298, https://doi.org/10.1016/j.enconman.2017.12.089.
[56] B. Tahir, M. Tahir, N.A.S. Amin, Photo-induced CO_2 reduction by CH_4 /H_2O to fuels over Cu-modified g-C_3N_4 nanorods under simulated solar energy, Appl. Surf. Sci. 419 (2017) 875–885, https://doi.org/10.1016/j.apsusc.2017.05.117.
[57] Y. Yu, L. Piao, J. Xia, W. Wang, J. Geng, H. Chen, X. Xing, H. Li, A facile one-pot synthesis of N-La codoped TiO_2 porous materials with bio-hierarchical architectures and enhanced photocatalytic activity, Mater. Chem. Phys. 182 (2016) 77–85, https://doi.org/10.1016/j.matchemphys.2016.07.007.